UTILIZATION OF NOVEL ATOM SOURCES IN STUDIES OF SEMICONDUCTOR SURFACES

By

JOHN T WOLAN

A DISSERTATION PRESENTED TO THE GRADUATE SCHOOL
OF THE UNIVERSITY OF FLORIDA IN PARTIAL FULFILLMENT
OF THE REQUIREMENTS FOR THE DEGREE OF
DOCTOR OF PHILOSOPHY

UNIVERSITY OF FLORIDA

1998

This dissertation is dedicated to the memory of my grandfather, Joseph Anthony Delzingaro, lovingly known as "Pop". A simple man whose wisdom and love live on.

ACKNOWLEDGMENTS

I would like to thank Gar Hoflund for his guidance, friendship and introduction to SCUBA diving. The investment made will bring many returns, thanks Gar. I would also like to thank Charles Mount and Bill Epling for their patience and assistance given to me in the lab. I would especially like to recognize and thank my parents, John and Ann Wolan, and grandparents, Joe and Mary Delzingaro, for their loving support through good times and bad. To my friend, lover, confidant and wife, thank you Nancy for all the Happiness, Joy and Wonder you have brought into my life. Finally, to my Higher Power who made all this possible, I give thanks.

TABLE OF CONTENTS

		page
ACKNOWLEDGMENTS		iii
ABSTRACT		vi
CHAPTERS		
1	INTRODUCTION	1
	Overview	1
	Importance of III/V Materials	1
	III/V Substrate Surface Preparation	3
	Passivating Oxide Interface	4
	Literature Review	5
	Epitaxy of III/V Materials	5
	Atomic Hydrogen	6
	Atomic Oxygen	7
2	DEVELOPMENT OF ESD O- AND H-ATOM SOURCES	10
	Design Approach	10
	Adsorption and Permeation	10
	ESD	11
	Design Considerations	11
	Operating Characteristics	12
	Neutral Atom Detection	13
	Flux Quantification	13
3	CHARACTERIZATION STUDY OF GaAs(001) SURFACES USING ION SCATTERING SPECTROSCOPY AND X-RAY PHOTOELECTRON SPECTROSCOPY	15
	Experimental	15
	Results and Discussion	16
	Summary	22
4	CHEMICAL REACTIONS INDUCED BY THE ROOM-TEMPERATURE INTERACTION OF HYPERTHERMAL ATOMIC HYDROGEN WITH THE NATIVE OXIDE LAYER ON GaAs(001) SURFACES STUDIED BY ISS AND XPS	29
	Experimental	29
	Results and Discussion	30
	Summary	34

5 CHEMICAL ALTERATIONS OF THE NATIVE OXIDE LAYER ON InP(111) BY THE EXPOSURE TO HYPERTHERMAL ATOMIC HYDROGEN 41

Experimental 42
Results and Discussion 42
Summary 48

6 ROOM TEMPERATURE OXIDATION OF A GaAs(001) SURFACE INDUCED BY THE INTERACTION OF HYPER-THERMAL ATOMIC OXYGEN STUDIED BY XPS AND ISS 56

Experimental 56
Results and Discussion 57
Summary 60

REFERENCES 66

APPENDICES

A ATOMIC OXYGEN FLUX QUANTIFICATION 71

B MODIFIED ALGORITHM USED TO CALCULATE THE OXIDE THICKNESS GROWN 73

BIOGRAPHICAL SKETCH 75

Abstract of Dissertation Presented to the Graduate School
of the University of Florida in Partial Fulfillment of the
Requirements for the Degree of Doctor of Philosophy

UTILIZATION OF NOVEL ATOM SOURCES IN STUDIES OF SEMICONDUCTOR SURFACES

By

John T. Wolan

August 1998

Chairman: Gar B. Hoflund
Major Department: Chemical Engineering

Nanometer-scale characterization of semiconductor surfaces is very important for precise control of the ultrafine structures necessary for the realization of devices using quantum confinement. The performance of these heterojunction devices is strongly dependent on interface quality. In the case of III-V semiconductors, the major problem is the presence of the native oxide layer and surface carbon contamination. This carbon is strongly bonded to the III-V surface even after ion-etching and high temperature annealing and induces a free-carrier depletion region at the substrate-epilayer interface. Furthermore, native oxides on GaAs and InP surfaces are detrimental to the formation of stable interfaces and can result in defective epitaxial growth, inducing undesirable electrical characteristics to the device so they must be removed without damaging the near-surface region.

A surface characterization study using ion scattering spectroscopy (ISS) and X-ray photoelectron spectroscopy (XPS) has been performed on GaAs(001) and InP(111) substrates before and after cleaning by ion sputtering/annealing cycles and room temperature exposure to the flux produced by a novel atomic hydrogen source based on electron-stimulated desorption (ESD) to determine any treatment induced alterations.

In order to realize high performance III-V circuits, the preparation of a good quality passivating oxide interface is necessary. Device quality oxide-(III-V) interface fabrication will certainly depend on the composition of the oxide interface and any possible damage induced by the oxidation process. In the case of GaAs, thermal oxides and formation of thick oxides (which actually is diffusion-controlled and possibly close to thermal equilibrium) usually results in non-stoichiometric films of Ga_2O_3 and As_2O_3 as well as a pile-up of elemental As at the GaAs-oxide interface. This structure is predicted by the Ga-O-As phase diagram, but it provides poor electrical isolation and surface protection (1).

In this study a novel hyperthermal oxygen atom source has been used to form an oxide layer on an Ar^+ sputtered GaAs(001) surface at room temperature, and this layer has been examined using X-ray photoelectron spectroscopy (XPS) and ion scattering spectroscopy (ISS).

CHAPTER 1
INTRODUCTION

Overview

The development of the solid-state electronics industry has principally centered around the semiconductor material Si, mainly as a result of its low cost, ease of preparation, available high-purity, and excellent native oxide passivation. To achieve better performance and higher packing density of integrated circuits, there has been a trend to down-size the device and circuit elements. Since the rate of voltage down scaling has not kept pace with the shrinking dimensions, increasingly higher electric fields are being applied to the successive generations of smaller devices. Although silicon has satisfied a large number of the requirements for solid-state device applications, there exists no degree of freedom in the inherent electrical properties of this material. In addition, the use of silicon for photonic, optoelectric and high-speed device applications (e.g., Light Emitting Diodes (LEDs), lasers, infrared detectors, Field Effect Transistors (FETs), and low-noise integrated circuits) is limited by the fundamental material properties of silicon. Due to the inflexibility and limitations presented by silicon, a considerable amount of research has focused on the development of alternative semiconductor materials to meet the demands of next generation devices.

Importance of III-V Materials

In particular, Group III-V compounds and solid solutions are receiving intense investigation. The motivation for the research resides in two principal advantages offered by III-V materials: the existence of three degrees of freedom in the properties of the material and improved inherent electrical properties. The first degree of freedom is found in the choice of the base binary system (nine possible compounds with the Group III elements Al,

Ga, and In and the Group V elements P, As, and Sb). While the second and third degrees of freedom are realized as a result of the ability to often form completely miscible substitutional solid solutions on both the Group III and the Group V sublattices independently. Thus, for example, it would be possible to specify a lattice parameter, bandgap energy and thermal conductivity (within a certain range) to satisfy the constraints for a given device structure. This point is illustrated in Figure 1.1 which plots the lattice parameter of III-V binary compounds versus the observed room temperature bandgap. The solid dots represent binary compounds and the lines connecting each dot represents ternary solid solutions of the two binary limits. Solid lines signify direct bandgap materials while broken lines indicate indirect materials. Essentially, the entire area enclosed in Figure 1.1 is accessible to the designer when employing ternary and quaternary III-V solid solutions.

The second advantage III-V materials offer is a general improvement in electrical properties over silicon. Table 1.1 illustrates some measured room temperature electron mobilities, bandgap energies and lattice parameters observed for III-V compounds and for Si (1).

This summary indicates that as much as two orders of magnitude improvement in speed and/or frequency can be realized with the use of III-V compounds over Si. Unlike Si, III-V materials are available in semi-insulating form which greatly reduces parasitic capacitances and allows the use of true monolithically integrated circuits that operate above 1 *GHz*. Considerable interest has been devoted to III-V semiconductor optoelectric device, such as buried heterostructure lasers, fabricated entirely by molecular beam epitaxy (MBE). Thus, III-V materials are expected to play an increasing role as the host materials for high-speed quantum effect devices. However, the widespread use of these materials is currently limited mainly due to poor interface quality and unsuitable native oxide passivation.

III-V Substrate Surface Preparation

The fabrication of such devices involves some critical intermediary technological steps. In order to obtain high-quality films by MBE, an atomically smooth and clean substrate surface is essential. Native oxides and surface carbon contamination can impede the growth of epitaxial layers and can contribute to undesirable electrical characteristics of the device so they must be removed without damaging the near-surface region. When classical *ex situ* cleaning methods are used, a carrier concentration depletion layer is observed at the growth interrupted interface. This carrier depletion is believed to originate from carbon and oxygen impurities accumulated on the substrate during chemical treatments and air exposure. Conventional *in situ* techniques to clean III-V semiconductor surfaces have relied upon ion bombardment and/or high temperature thermal desorption/annealing. Such methods often result in residual damage or depletion of the more volatile Group V element. Other techniques based on reactive gas etching have been proposed for the cleaning of III-V surfaces. These include rf hydrogen plasma etching, thermal etching in a HCl H_2 mixture, cleaning with a hydrogen-radical beam generated by an electron cyclotron resonance (ECR) plasma. These methods have disadvantages. The ECR sources are expensive and physically incompatible with standard MBE systems. Furthermore, the energized particles generated by the above mentioned techniques can damage the substrate surface. An atomic-hydrogen source based on the principles of thermal cracking also has been investigated. The hot tungsten filament used to crack the H_2 heats both the source and the sample operating at temperatures as high as 2400°C with a resulting chamber pressure > 6.0×10^{-6} Torr. Therefore, new techniques for III-V surface cleaning prior to epitaxial growth are needed to eliminate or minimize the resulting interface depletion region.

Passivating Oxide Interface

In order to realize high performance III-V circuits the preparation of a good quality passivating oxide interface is necessary. Generation of a well-defined substrate/overlayer interface is complicated by the dependence of the surface composition on the different reactivities of the Group III and Group V elements. There are a number of approaches for III-V oxidation which have been of major interest in recent years. Device quality oxide-(III-V) interface fabrication will certainly depend on the stoichiometric composition of the oxide interface and any possible damage induced by the oxidation process. In the case of GaAs, thermal oxides and formation of thick oxides (which actually is diffusion-controlled and hence close to thermal equilibrium) usually results in non-stoichiometric films of Ga_2O_3 and As_2O_3 as well as a pile-up of elemental As at the GaAs-oxide interface. This structural composition which is mostly found in many oxidation processes is clearly predicted by the Ga-O-As phase diagram, but provides poor electrical isolation and surface protection.

Application of an oxygen plasma in the vicinity of GaAs-MOS structures is not desirable because it results in a departure from surface stoichiometry, the likely causes of a high density of interface states. Although indirect-induced plasma processes may systematically avoid disturbing the III-V surface, the growth of plasma-induced oxides still results in a Group-III deficient interface. The UV/ozone oxidation processes have been widely established for pre-epitaxial surface preparation. In principle, higher oxidized states of As and Ga are formed under the influence of light at low substrate temperatures (below 100°C). However, oxide composition is dependent on the wavelength applied and the time exposed. The UV wavelengths of interest are 184.9 nm and 253.7 nm. The first wavelength is absorbed by O_2 producing O_3 which reacts with carbon atoms on the III-V surface forming CO_2, thus reducing carbon contamination. The latter wavelength is absorbed O_3 forming O_2 and atomic oxygen which leads to an oxidation of the III-V surface. A comparison of structure and composition of the oxide-(III-V) interface has led

to the conclusion that UV/ozone oxidation involves a rather complex process in view of controlling oxide and interface properties. In the case of other oxidation techniques such as chemical, anodic, ion beam- and electron beam-induced oxidation, disadvantages can easily be identified. Surface contamination related to adatoms remaining on the III-V surface, structural alterations, changes in surface stoichiometry and charging effects due to electron or ion bombardment have all been cited.

Literature Review

Epitaxy of III-V Materials

Considerable interest has been devoted to III-V semiconductor optoelectric devices, such as buried heterostructure lasers, fabricated entirely by MBE. These compound semiconductor materials exhibit many desirable properties including high carrier mobilities and densities and large bandgaps, which often are tunable. For these reasons they show promise for high speed quantum effect devices (2-6). Nanometer-scale characterization of GaAs surfaces is very important for precise control of the ultrafine structures necessary for the realization of devices using quantum confinement. In order to obtain high-quality films by MBE, a substrate that is smooth and clean on the atomic scale is a prerequisite (7). The performance of these heterojunction devices is strongly dependent on interface quality. Impurities on the substrate surface can interfere with the initial nucleation inducing roughening and surface states which degrade the device performance (8-12). In the case of III-V semiconductors and particularly for GaAs, the major problem is the surface carbon contamination and the presence of the native oxide layer and surface carbon contamination. This carbon is strongly bonded to the III-V surface even after ion-etching and high temperature annealing and induces a free-carrier depletion region at the substrate-epilayer interface (13). The mechanism causing these interface states is not clear. For GaAs it is certain that these states are related to carbon contamination of the crystal surface during air exposure (14). Native oxides on GaAs surfaces are detrimental to the formation of stable

interfaces and can result in defective epitaxial growth, inducing undesirable electrical characteristics to the device

Atomic Hydrogen

Utilization of atomic hydrogen in MBE offers many potential benefits in substrate preparation and resulting material quality. Low-temperature cleaning of GaAs, InP and Si substrates (8,14-20), surfactant-assisted epitaxy (21,22), selective epitaxy and passivating the electrical activity of donors and deep levels in GaAs (23,24) have all benefited from the addition of atomic hydrogen. In MBE the cleaning of substrate surfaces is very important from the standpoint of obtaining high-quality epitaxial films. To remove contaminants from the GaAs substrate surface, ion- or plasma-beam etching and/or thermal etching is typically used. Recently, atomic hydrogen has been studied as a new low-temperature cleaning method of GaAs surfaces. Many of these studies are based on the use of electron-cyclotron-resonance (ECR) sources to generate the *H* flux (8,14,15,25). However, these sources are expensive and physically incompatible with standard MBE equipment. Furthermore, they generate energized particles which can damage the substrate. An atomic-hydrogen source based on the principles of thermal cracking also has been investigated (8,17,19,21,22,27-30). This thermal cracker is similar to those used to crack arsine and phosphine but modified so as to produce the high temperature (> 1600°C) needed for cracking H_2. This method has disadvantages. The hot tungsten filament heats both the source and the substrate, and the best cracking efficiency to date is < 20% at temperatures as high as 2400°C with a resulting chamber pressure > 6.0 x 10-6 Torr (31)

Various cleaning procedures have been investigated in the past, and it appears that the chemical nature and structures of III-V surfaces vary significantly with the cleaning method used (32-34). Standard surface cleaning procedures are (i) wet chemical etching and mechanopolishing which are ex-situ procedures not able to completely remove carbon and oxygen contamination, (ii) thermal desorption in an overpressure of Group V species

or compound to suppress incongruent evaporation, and (iii) ion sputtering and annealing which can lead to lattice disruption as much as 100 nm below the surface (20)

Atomic Oxygen

A source of hyperthermal (several electron volts) oxygen atoms with a significant flux (> 10^{14} atoms cm^{-2} s^{-1}) would be useful in many application areas including the growth of compound semiconductor materials by MBE. During the growth of compound semiconductors, it is often required to produce insulating oxide layers This may be difficult to impossible using O_2 because the sticking coefficient of O_2 on III-V semiconductors and other materials is often very low This problem could be overcome by using O-atoms, which most likely have a sticking coefficient of ~ 1 to form the oxide layers (35)

Table 1.1. Some Properties of Si and III-V Binary Semiconductors at 300K

	Bandgap (300 K)		Electron Mobility at (300 K) (cm2/V S)	Lattice Constant (Å)
	Type	Energy (eV)		
Si	indirect	1.12	1500	5.43
InSb	direct	0.17	80000	6.48
InAs	direct	0.36	33000	6.06
GaSb	direct	0.72	5000	6.10
InP	direct	1.35	4600	5.87
GaAs	direct	1.42	8500	5.65
GaP	indirect	2.26	110	5.45
GaN	direct	3.36	380	a = 3.19, c = 5.18

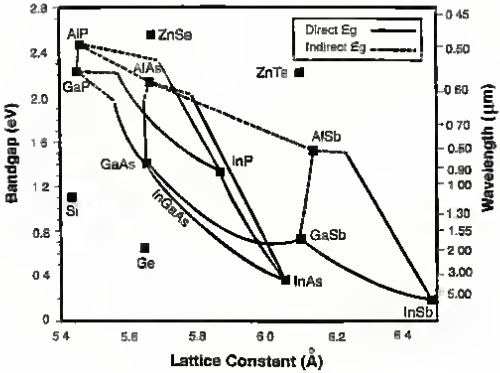

Figure 1.1 Plot of the lattice parameter of III-V binary compounds versus the observed room temperature bandgap

CHAPTER 2
DEVELOPMENT OF ESD O- AND H-ATOMS SOURCES

Design Approach

The operational concept of the hyperthermal atom generator (HAG) is shown in Figure 2.1 using the O-atom source for illustrative purposes, but the same concept also applies for the H-atom source. An ultrahigh purity molecular gas (e.g., oxygen or hydrogen) dissociatively adsorbs on a metallic membrane at the high pressure side and diffuses at elevated temperature (> 400°C) to the ultrahigh-vacuum (UHV) side. Here the adsorbed atoms are struck by a directed flux of primary electrons which results in electron stimulated desorption (ESD) of atoms. Many processes have to function in series at sufficiently high rates for the system to work. These include dissociative adsorption of the molecular gas on the metal surface, diffusion of atoms through the membrane and formation of the neutral flux by ESD. In these sources the membrane materials and operating parameters are dependent upon the molecular gas precursor used.

Adsorption and Permeation

The rates of adsorption of the gas on the high-pressure side of the membrane and the permeation through the membrane must be at least as high as the neutral flux. This condition determines the minimum pressure upstream of the membrane and the operating temperature of the membrane. As an example, for O_2 adsorption on Ag at 400°C, the sticking coefficient may be as low as 10^{-6} so an upstream pressure of at least 1 Torr is required to produce a flux above 10^{14} atoms/cm^2-s. The permeability of the membrane is the product of solubility and diffusivity, and varies exponentially with temperature similarly to the diffusivity. We have measured the permeation rate of O through Ag over the temperature range 400-800°C (36) and found it to be linear below 630°C and repeatable. A

break occurs in the Arrhenious plot of diffusivity at 630°C due to thermal desorption of O_2 from the surface. Based on these data an operating temperature of 500°C was chosen because the permeation rate through the Ag membrane is high enough to produce the required flux and stable chemisorption layer of O-atoms is maintained at the surface, since the thermal desorption rate of O_2 is very low and the evaporation rate of Ag is negligible at this temperature.

ESD

Electron stimulated desorption is a complex process in which particles are emitted from a surface through decay of a localized electronic excitation created by an incident electron. The intensity of the desorbing particle flux can be expressed as [1]

$$\frac{I}{A\varepsilon} = \frac{I_p}{A\varepsilon} Q(N) \qquad [1]$$

where I_p is the total electron beam current to the membrane, A is the irradiated area of the membrane, ε is the charge on an electron, Q is the ESD cross section and (N) is the surface concentration of adsorbed neutrals (37). In order to maximize the ESD flux, it is necessary to maximize both I_p and (N) by optimizing the source operating parameters unique to the chemical system being used.

Design Considerations

As shown in Figure 2.1, the primary electron beam current to the membrane is produced by a circular filament and reflector around the perimeter of the membrane. Ideally, the emission current produced by this filament should be the limiting factor. In addition to providing the primary electron beam flux for ESD, this filament also provides the power input to the source which keeps the membrane at its operating temperature. It is necessary to design the membrane support assembly to maximize heat transfer away from

the membrane so that the filament emission current can be set between 30 and 60 mA. It is important that this current be spread across the membrane as uniformly as possible to maximize the atom flux and minimize damage to the membrane by formation of hot spots. This has been accomplished using the SIMION computer program (38)

The membrane material is an important consideration for each type of atom produced. Pure metals and alloys can be used, and each composition results in a different adsorption rate, permeation rate, ESD cross section, operating temperature and primary electron beam voltage. The power input is equal to the primary beam current multiplied by the voltage. The voltage for any membrane material is chosen to optimize the ESD cross-section so this voltage times the filament emission current yields the power input to the source and, hence, the amount of heat which must be removed from the source by a combination of radiative, convective and conductive heat transfer The heat transfer resistances must be designed to keep the membrane at the appropriate operating temperature for that particular material. Many different membrane materials can be utilized for each different type of atom produced including pure metal and alloys of: Ag, Zr and Ti for O-atoms; Pd, Zr, Ni, Cu and Ti for H atoms; and Zr, Ta and Fe for N atoms. All of the source parameters are different for each type of membrane used. The purity of the atom flux and the UHV compatibility are very important considerations. Since the atom sources operate at elevated temperatures, they outgas, and the outgassing rate can be reduced by using a cooling water or LN_2 shroud to keep most of the components cool. In a typical MBE system, the pressure with the source operating is 10^{-9} Torr or below

Operating Characteristics

The atom fluxes produced by the source are well characterized and very high purity. If the membrane temperature is too high then the molecular desorption can occur as membrane material can be evaporated. The average energies of the neutral fluxes produced range from 1 to 3 eV, and this flux is linearly dependent upon emission current. The

neutral-to-ion ratio typically is about 10^6 so the relatively few ions produced can usually be neglected. The atoms produced are in their ground states. It is possible to pulse the primary electron flux so that time-dependent experiments can be performed.

Neutral Atom Detection

Since neutral ESD species are difficult to detect, very few ESD studies of neutral species have appeared in the literature. Our research group developed an experimental ESD system capable of detecting emitted neutrals (39). The neutral atoms are detected by operating a quadrupole mass spectrometer (QMS) in the appearance potential (AP) mode to allow the atoms to be distinguished from residual gases and background gas products formed by collisions of the neutrals with the walls of the system. In the AP mode the energy of the ionizing electrons is reduced below the first ionization potential of the background species to accentuate the neutral signal.

Flux Quantification

Measurement of an atom flux is a challenging problem because neutral detection is quite difficult and sensitivity factors needed for quantification have to be determined. Three different methods have been developed and described for measuring the atom flux (40). The first is to use the QMS, as described above, in the AP mode to directly measure the intensity of the neutral signal. The second is to expose a Pt foil to the atom flux for a given period of time and measure the atom coverage using ion scattering spectroscopy (ISS). The third method is to determine the ESD primary beam current, estimate the membrane atom coverage and calculate the atom flux using the previously determined neutral cross section (41). Agreement between the results obtained from the three methods is excellent. The data and calculation method used in the Pt ISS study is presented in Appendix A.

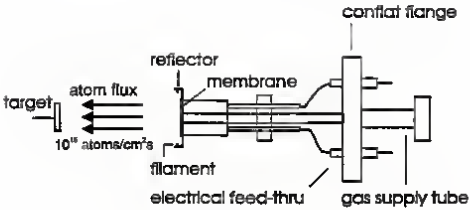

Figure 2.1. Schematic diagram of the atom source.

CHAPTER 3
CHARACTERIZATION STUDY OF GaAs(001) SURFACES USING ION SCATTERING SPECTROSCOPY AND X-RAY PHOTOELECTRON SPECTROSCOPY

In order to use the GaAs surface for the fabrication of ultrafine structures, a complete understanding of the surface morphology and topography before and after surface treatment is essential. Typically, in device manufacturing based on single crystal epitaxy, an air exposed, polished and organic solvent cleaned GaAs(001) surface is further treated by *in-situ* sputter etching and annealing. Therefore, this study was undertaken to obtain detailed compositional and chemical-state information regarding these surfaces and any treatment-induced alterations.

Outermost and near-surface compositions of polished, air-exposed, solvent-cleaned and sputtered/annealed *n*-type (Si, ~3 x 10^{18} cm^{-3}), GaAs(001) substrates have been examined using ISS and X-ray photoelectron spectroscopy (XPS). The data indicates that the native oxide layer is complex chemically. It contains a significant amount of carbon as well as hydrogen (42) which is usually ignored due to difficulty in detection. Ion sputtering and annealing cycles is a drastic treatment resulting in significant changes at the surface, which have been examined in this study. These results may lead to improved methods for cleaning GaAs surfaces for growth.

Experimental

The as-received Sumitomo Industries Ltd., Si-doped, *n*-type GaAs(001) substrate with a carrier concentration of approximately 3 x 10^{18} cm^{-3} was ultrasonically solvent cleaned in toluene, acetone, trichloroethylene, acetone and ethanol (in that order) and then inserted into the ultrahigh-vacuum (UHV) chamber (base pressure of 10^{-11} Torr). X-ray photoelectron spectroscopy and ISS were performed using a double-pass cylindrical mirror

analyzer (CMA) (PHI Model 25-270 AR). The XPS data were taken in the retarding mode with a pass energy of 25 eV using Mg Kα X-rays (PHI Model 04-151 X-ray source). Data collection was accomplished using and a computer interfaced, digital pulse counting circuit (43) followed by smoothing with digital filtering techniques (44). Ion scattering spectroscopy was carried out in the nonretarding mode using a defocused primary beam of high purity 1-keV Ne^+ at a current of 100 nA over an area approximately 0.5 cm in diameter. A scattering angle of 137 ± 6° was used and a spectrum was collected in about 90 s. For each sample examined XPS was performed first followed by ISS in order to avoid sample damage before collection of the XPS data. Ion scattering spectroscopy removes surface species by ion sputtering resulting in compositional changes of the III-V surfaces. Sample damage has been minimized in this study by exposing the sample to the beam for the minimum period required to obtain reasonable signal-to-noise ratios. Since both ISS and XPS were performed using defocused sources, the ISS and XPS data represent an average over the area analyzed.

Results and Discussion

The XPS and ISS spectra were obtained first from as-received solvent-cleaned samples. Gallium arsenide (001) surfaces next were sputtered with 1-keV Ar^+ sputter and annealed in cycles until no O 1s peak was observed in XPS. Ion scattering spectroscopy was then performed after cleaning, heating to 180°C and cooling to room temperature. A clean GaAs(001) surface was sputtered for 30 minutes with 1-keV Ne^+ and finally ISS was performed in 5 minute increments to observe any surface alterations with time. Annealing was performed by heating the back of a titanium foil support radiatively with a tungsten filament approximately 0.5 cm from the sample holder. The substrate temperature was determined by using a chrome alumel thermocouple which was in contact with the sample.

The XPS survey spectra obtained from an as-entered, solvent-cleaned GaAs(001) surface before and after 1-keV Ar^+ sputter and anneal cycles are shown in Figure 3.1a and

b, respectively The survey spectrum obtained after elimination of the O 1s peak is shown in Figure 3 1c Significant changes in peak shapes and relative peak heights are observed for Ga, As, C and O The O 1s peak in Figure 3.1a is predominant since a large amount of O is present initially and the O 1s sensitivity factor is larger than those of the peaks shown for other species present. The C 1s peak is of particular importance. Its size decreases with the cleaning treatments, but it is still evident after the O 1s peak essentially is eliminated. A small amount of carbon contamination at the oxide-GaAs interface is known to affect the electrical properties of epitaxial layers. The carbon-related defects have been observed to propagate into the epitaxial overlayer Furthermore, Kawai, Wood and Eastman (44) have reported that surface carbon phases can survive temperatures that exceed the decomposition temperatures of the GaAs substrate.

Using the homogeneous assumption and published sensitivity factors (45), the composition of these surfaces could be calculated. However, these surfaces are known to consist of a thin oxide layer over the GaAs substrate, and the oxide layer apparently is layered similarly to the native-oxide layer on InP substrates (32-34,46) This matrix effect (geometrical distribution of the near-surface species) can result in very large errors as demonstrated by Hoflund and Minahan (47) so compositions have not been calculated using the homogeneous assumption.

High-resolution XPS As 3d, Ga 3d, O 1s and C 1s spectra obtained from an as-entered, solvent-cleaned GaAs(001) substrate before (a) and after 1-keV Ar^+ sputter and anneal cycles (b) are shown in Figures 3.2 and 3.3. Significant variations in the peak shapes and positions are observed between a and b in all sets of spectra indicating that the nature of the chemical species present is altered significantly by sputtering and annealing. The As and Ga 3d peaks shown in Figure 3 2a indicate that As_2O_5, As_2O_3, Ga_2O_3 and GaAs all are present in the near-surface region on the as-entered sample. The asymmetrical shape on the high binding-energy side of the As 3d peak suggests that some elemental arsenic may be present. The spectra shown in Figure 3 2b and 3.3b correspond to the

survey spectrum shown in Figure 3 1c obtained from the cleaned sample. The feature due to As oxides is not present, but a small Ga_2O_3 contribution in the Ga 3d peak is apparent as a shoulder on the high binding-energy side of the Ga 3d peak. This result suggests that Ga_2O_3 lies beneath the As oxides, which is consistent with the findings of Röhkel and Hartnagel (48). A calculation was performed using spectrum a to determine the ratios of As bonded as oxide to As present as GaAs and As^0 and Ga bonded as oxide to Ga present as GaAs and Ga^0. These ratios are 0 45 and 1 03 indicating that the oxide layer is Ga oxide rich containing more than twice as much Ga as As. A model can be proposed for the oxidation of GaAs which is consistent with these data. In this model both Ga and As are oxidized initially As the oxidation proceeds Ga migrates to the surface forming Ga_2O_3 leaving an As-rich layer beneath the oxide layer Therefore, the layered structure consists of a mixture of Ga_2O_3, As_2O_3 near the surface. Below this lies a Ga_2O_3-rich region, and just under the oxide layer lies an As^0-rich region above bulk GaAs. The proposed model is also consistent with the Ga-As-O phase diagram estimated by Thurmond et al. (49) from a combination of experiments and free energy calculations.

The O 1s peak shapes shown in Figure 3.3A also vary significantly before and after cleaning The O 1s feature is broad initially and consists of contributions from both As and Ga oxides. The O 1s feature obtained after cleaning is reduced to a very small peak just above the noise level. The As oxide contribution is no longer present, but a peak due to Ga_2O_3 still is apparent. Most of the O present is of some other form such as chemisorbed O or a subsurface dissolved O with a BE of about 529 0 eV. In studies of AgO and Ag_2O, chemisorbed O has a BE of 528.2 eV and subsurface dissolved O has a BE of 531.0 eV. This suggests that the low-BE O 1s feature in Figure 3 3Ab is due to chemisorbed O

The C 1s peak shapes shown in Figure 3 3B are quite complex and are changed significantly after cleaning. Peaks or shoulders due to several different carbon species are apparent at 283 2, 284 6, 286 0, 287 8 and 289 4 eV Carbon has a relatively small sensitivity factor so the C 1s peak heights in Figure 3 1 indicate that relatively large

amounts of C are present at this surface The spectrum obtained from the solvent-cleaned surface shown in Figure 3 3Ba exhibits a predominant peak at 284 6 eV due to the presence of hydrocarbons. A shoulder is present at a BE of 287 8 eV possibly due to adsorbed species such as Me_2CO, and a shoulder is present at 286.0 eV due to the presence of adsorbed alcohols A very small amount of bicarbonate may be present yielding a small peak at 289 4 eV Another shoulder is present on the low-BE side which is most likely due to the presence of Ga carbide. Neither Ga carbide nor As carbide are known to exist as bulk compounds. However, III carbides such as Al_4C_3 are known to exist whereas V carbides have not been synthesized or identified. C 1s features with BEs below 284 0 eV are due to carbides. Based on these facts the carbide features observed in this study are believed to be due to Ga carbide. After sputtering/annealing treatments the predominant form of C is carbide, but small shoulders due to hydrocarbons and alcohols also are present. In Figure 3 1c, the O 1s peak is decreased in size until it nearly is eliminated by the sputtering/annealing cycles, but the C 1s peak remains large. This is due to the fact that it is converted to a carbide, which is very difficult to remove. These data imply that a cleaning technique should be developed which simply removes the hydrocarbons rather than converting it into carbide which is so difficult to remove. The mechanism through which hydrocarbon is converted to carbide by ion sputtering is not understood. It may involve breakage of the H-C bonds, selective sputtering of H and bonding of C to Ga as a carbide.

Although carbon contamination is nearly always present on air-exposed surfaces, very little is known about the structure or composition of this carbon so the C 1s peak should not be used as a BE reference, which has been standard practice in XPS studies. In this case the C 1s spectrum in Figure 3.3Ba has a complex shape, but the predominant peak is due to hydrocarbons so the spectra obtained from the as-entered sample could be shifted based on the C 1s feature. However, this would not work for the spectrum obtained from the cleaned surface because the predominant feature is due to Ga carbide.

The Ga(LMM) Auger peaks shown in Figure 3.1 are also changed significantly after cleaning. The $Ga(L_3M_{4,5}M_{4,5})$ and $Ga(L_1M_{2,3}M_{4,5})$ features at BEs of approximately 190 and 282 eV show a dramatic increase with cleaning. High resolution XPS spectra shown in Figure 3.3B clearly illustrate the increase $Ga(L_3M_{2,3}M_{4,5})$ peak in the C 1s binding energy region.

The high surface sensitivity of ISS makes it a very important surface analytical tool capable of yielding compositional information about the outermost atomic layer of a solid. This is important because surface chemical processes such as film growth and cleaning occur at the outermost atomic layer even though the subsurface regions are altered by migration of species participating in the reaction. ISS is most useful for providing complimentary information to XPS and Auger electron spectroscopy (AES). These techniques are much less surface sensitive. Generally, they probe more than 30 atomic layers beneath the surface and less than 10% of the total signal originates from the outermost atomic layer. This information from the outermost atomic layer usually cannot be separated from the subsurface layer information so ISS provides very important, complementary information to these more commonly used techniques.

The principle features in ISS are due to elastic scattering of inert-gas ions (usually He^+ or Ne^+) off the solid surface. Detailed descriptions of the ISS process have been published (50-55) and are not reviewed here. Ion scattering spectroscopy is so highly surface sensitive because both the scattering cross sections and the neutralization probability are large. Primary ions which penetrate beneath the surface either are neutralized or scatter multiple times losing energy in each collision and finally contribute to the background. The neutralization probability is influenced by the electrical properties of the surface, i.e., for conductors the ion background is very small whereas it is large for less conductive surfaces.

Ion scattering spectroscopy spectra obtained using 1-keV Ne^+ from the as-received, solvent cleaned surface before and after sputter cleaning and annealing are shown in

Figures 3 4a and b respectively The ISS peaks due to the Ga and As appear at E/E_0 values of 0 340 and 0 365 respectively for the scattering angle used in this study These E/E_0 values are in excellent agreement with the binary elastic collision scattering equation. A significantly higher Ga-to-As ratio on the solvent-cleaned surface is evident compared to the clean surface. These ISS spectra are in good agreement with those obtained by Röhkel and Hartnagel (48) before and after cleaning a GaAs(100) surface by ion sputtering. The peak located at an E/E_0 of 0.422 is attributed to multiple scattering events between the target atoms and the incident ion beam. The shape of this feature is determined by the structural arrangement of the atoms at the surface (56) so it changes with the various treatments. A large background signal is evident in Figure 3 4a relative to that of the cleaned surface. The decrease in the background is due to the surface becoming more conductive as the insulating oxide layer is removed. Peaks due to C or O do not appear in ISS spectra taken with Ne^+ at the scattering angle used because they are lighter than the primary ion (50).

Ion scattering spectroscopy spectra taken after heating the cleaned surface to 180°C and then cooling to room temperature are shown in Figures 3.5a and b, respectively The Ga-to-As atom ratio is larger at 180°C than at 32°C by about 15% Since 180°C is well below the sublimation temperature for As (> 600°C), the increased Ga at the outermost surface is presumed to be due to migration of subsurface Ga atoms to the outermost layer. The increase in the inelastic scattering peak can be attributed to alterations in the surface structure. These results were both reproducible and reversible.

The ISS spectra obtained from a clean GaAs(001) surface immediately after sputtering for 30 minutes with 1 keV Ne^+, the same surface after waiting 10 min and then another 120 min are shown in Figure 3 6a, b and c, respectively The surface Ga-to-As ratio decreases by a small amount as the surface relaxes after the ion-etch This result demonstrates that these surfaces change slowly after ion sputtering. Initiating epitaxial growth on GaAs(001) immediately after ion sputtering may result in atomic rearrangements at the film-substrate interface which could influence the structure and properties of the film.

Summary

The XPS and ISS have been used to examine the outermost and near-surface regions of polished, air-exposed, solvent-cleaned, n-type ($S_i \sim 3 \times 10^{18}$ cm^{-3}) GaAs(001) substrates before and after cleaning by cycles of ion sputtering and annealing treatments. The native oxide layer on the solvent-cleaned GaAs(001) substrate contains large amounts of C, As_2O_5, As_2O_3 and Ga_2O_3 according to the XPS data. Several forms of C are present including hydrocarbons, alcohols and carbide, but hydrocarbons are predominant. The XPS data indicates that the native oxide layer contains considerably more Ga oxide than As oxide. Furthermore, the As oxides are removed by ion sputtering at a lower total ion dose than Ga oxide which also is consistent with the fact that less As oxide is present. The data obtained in this study lead to the suggestion that the native oxide formed on air-exposed GaAs(001) surfaces is layered. The outermost region consists of a mixture of Ga and As oxides. Gallium (III) oxide is the only oxide present near the interface, and elemental As lies just beneath the native oxide layer and above the bulk GaAs. The native oxide layer contains a significant amount of C mostly in the form of hydrocarbons. Ion sputtering converts the hydrocarbons into Ga carbides which are very difficult to remove. *In-situ* sputter etching and annealing treatments result in significant changes in the surface Ga-to-As atom ratios. The Ga concentration in the outermost atomic layer is about 10% greater than the As concentration according to ISS data obtained from the solvent-cleaned surface. The large background indicates that this surface is nonconductive. The Ga-to-As surface atom ratio determined using ISS increases by annealing at temperatures as low as 180°C. A sputter-cleaned surface exhibits an increase in the Ga-to-As surface atom ratio which returns to the initial ratio with time as observed by ISS.

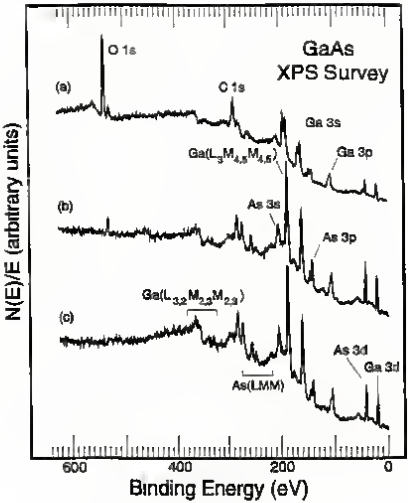

Figure 3.1. XPS survey spectra obtained from a solvent-cleaned, GaAs(001) substrate (a) as-entered, (b) after several 1 keV Ar^+ sputter and anneal cycles and (c) after continued cycles until no oxygen was observable in the survey spectrum. Peak assignments shown pertain to all three spectra.

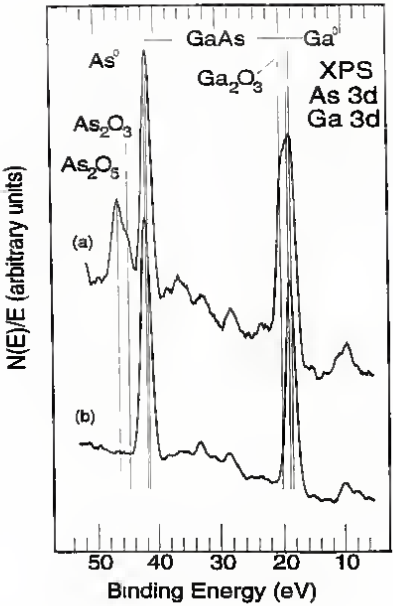

Figure 3 2. XPS Ga and As 3d spectra obtained from a solvent-cleaned, GaAs(001) substrate (a) as-entered and (b) after 1-keV Ar^+ sputter and anneal cycles corresponding to the spectrum shown in Figure 2 1a.

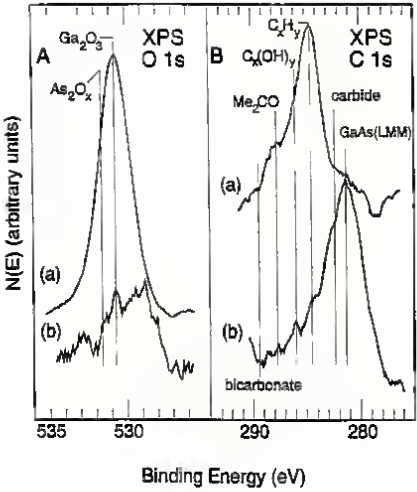

Figure 3.3 XPS (A) O 1s and (B) C 1s spectra obtained from a solvent-cleaned, GaAs(001) substrate (a) as-entered and (b) after 1-keV Ar^+ sputter and anneal cycles corresponding to the spectrum shown in Figure 2.1c

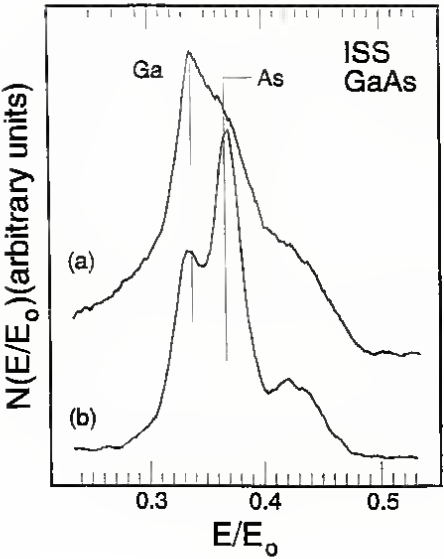

Figure 3.4. ISS spectra obtained from a solvent-cleaned GaAs(001) substrate (a) as-entered and (b) after 1-keV Ar^+ sputter and anneal cycles corresponding to the spectrum shown in Figure 2.1c.

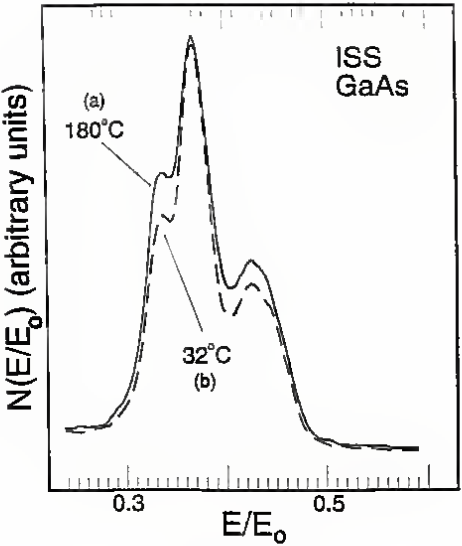

Figure 3.5 ISS spectra obtained from a solvent-cleaned GaAs(001) substrate after 1 keV Ar^+ sputter and anneal cycles corresponding to the spectrum shown in Figure 2.1c, (a) after heating the clean surface to 180°C and then (b) cooling to room temperature.

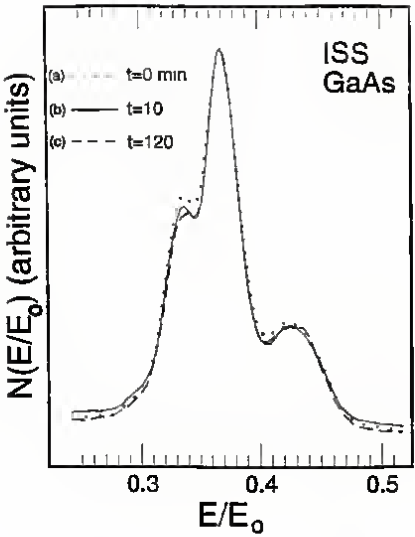

Figure 3 6. ISS spectra obtained from a solvent-cleaned, GaAs(001) substrate (a) after sputtering for 30 min with 1-keV Ne^+, (b) the same surface after waiting 10 min and then (c) 120 min after sputtering.

CHAPTER 4
CHEMICAL REACTIONS INDUCED BY THE ROOM-TEMPERATURE INTERACTION OF HYPERTHERMAL ATOMIC HYDROGEN WITH THE NATIVE OXIDE LAYER ON GaAs(001) SURFACES STUDIED BY ISS AND XPS

A surface characterization study using XPS and ISS has been performed on solvent-cleaned, n type GaAs(001) substrates before and after room-temperature exposure to the flux produced by a novel atomic hydrogen source based on ESD of hyperthermal (~1 eV) hydrogen atoms. The native oxide layer on the solvent-cleaned GaAs(001) substrate contains C, As_2O_5, As_2O_3 and Ga_2O_3 according to the XPS data with Ga_2O_3 being the predominant species. Before H-atom exposure the C is present as hydrocarbons, carbonates, alcohols and carbides with hydrocarbons as the predominant chemical state. Upon room-temperature exposure to a 1-eV hyperthermal H-atom flux, the O in As and Ga oxides is removed, and the amount of C present is reduced through methane formation and desorption. In this process hydrocarbons are not converted to carbides which are difficult to remove, as in the case of ion sputtering. After reduction the predominant form of O is a subsurface, dissolved O and the outermost atomic layer is enriched in O by a chemical-induced driving force.

Experimental

The details of the characterization experiments have been presented in the previous chapter. X-ray photoelectron spectroscopy and ISS spectra were obtained first from an as-received, solvent-cleaned sample. The sample was then transferred into an adjoining UHV chamber which houses the atom source via a magnetically coupled rotary/linear manipulator. The surface was then exposed to a 1-eV hyperthermal H flux and reexamined after total exposure times of 15 min, 45 min and 18 hr. At no time was the sample exposed to air after the initial insertion into the UHV chamber. The sample was maintained at room

emperature with a slight temperature increase (~50°C) due to exposure to the X-ray source during XPS data collection. The substrate temperature was determined using a chrome alumel thermocouple.

Results and Discussion

The XPS survey spectra obtained from an as-received, solvent-cleaned Ga(001) surface before and after a 15-min, H-atom exposure are shown in Figure 4.1a and b, respectively. Significant changes in peak shapes, positions and relative peak heights are observed for Ga, As, C and O. The O 1s peak in Figure 4.1 is predominant since a large amount of O is present initially and the O 1s sensitivity factor is larger than those of the peaks shown for other species present. Small features due to Cl, F and Na (not shown) are present at about the noise level. This is consistent with the ISS data discussed below. Relative to the O 1s peak, the Ga and As 3s, 3p, 3d and Auger peaks all increase in height with H-atom exposure and their peak shapes are changed due to reduction of As- and Ga-oxides. The C 1s peak is of particular importance. Its intensity decreases significantly with the cleaning treatment. The significant change in shape to the C 1s region is due to the facts that C is removed from the surface and that the $Ga(L_3M_{2,3}M_{4,5})$ feature becomes more prominent. The O 1s peak height still is quite large after the 15 min exposure, but continues to decrease in intensity with further treatment. In this study the O-to-Ga peak area ratio is decreased from 3.0 to 1.5, and the C-to-Ga peak area ratio is reduced from 3.0 to 1.4 during the H-atom exposures. These changes are due to both changes in the composition of the near-surface region and to changes in the matrix.

High-resolution XPS As 3d, Ga 3d, Ga 2p, O 1s and C 1s spectra obtained from an as-received, solvent-cleaned GaAs(001) substrate before and after exposure to the H-atom flux for various periods are shown in Figures 4.2 and 4.3. Significant variations in peak shapes and positions are observed between nonexposed and exposed surfaces in all of the spectra, indicating that the nature of the chemical species present is altered significantly

by exposure to the H atom flux. The Ga and As 3d levels are typically used for chemical state analysis, and the reference BEs used for these assignments are given in table 4.1. The As and Ga 3d peaks shown in Figure 4.2Aa indicate that As_2O_3, As_2O_5, Ga_2O_3 and GaAs are all present in the near-surface region of the as-received sample. As shown in Figure 4.2Ab, the features due to As oxides are eliminated by the 15 min. H atom exposure, but a small Ga_2O_3 contribution still is apparent as a shoulder on the high-BE side of the Ga 3d peak. This observation is consistent with data obtained in the previous study (56). The Ga 2p peak positions shown in Figure 4.2Ba and 4.2Bb also vary significantly before and after the H atom exposure. The Ga 2p BEs for Ga_2O_3 and GaAs are 1117.8 eV (57) and 1117 eV (58) respectively. The shift to lower BE after the 15 min H-atom treatment is consistent with oxide removal.

The O 1s peak shapes and positions obtained from the sample are shown in Figure 4.3A before and after incremental-time exposures to the H-atom flux. With increasing exposure the peak develops a more symmetrical shape and shifts toward lower BE. The O 1s feature is initially broadened toward the high BE side due to contributions from both As and Ga oxides. The As oxide shoulder decreases with exposure time. After the 18-hr treatment most of the O is present in some form other than As oxide or Ga oxide. It has an O 1s BE of about 530.2 eV and probably is a dissolved or interstitial atomic oxygen. In studies of AgO and Ag_2O (59,60), chemisorbed O has a BE of 528.2 eV and subsurface dissolved O has a BE of 531.0 eV. This fact is consistent with the assertion that the O 1s feature in Figure 4.3A after H atom treatment is due to subsurface dissolved O particularly since other forms of O have been removed. In the previous study of sputter cleaned GaAs(001), the remaining small O 1s feature is due to chemisorbed O with a BE of 529.0 eV.

The zincblende lattice of GaAs consists of two interpenetrating fcc sublattices, with the origin of the second sublattice located one fourth of the distance along the major diagonal of the first sublattice. The unit cube for GaAs has a volume a^3, where a is the

lattice constant. Each gallium (or arsenic) atom has four nearest neighbor arsenic (or gallium) atoms, with a bond length of $r_0 = 3^{0.5} a/4$. These bonds are separated by the tetrahedral bond angle of 109.47°. Any deviation in a crystal from a perfect periodic lattice or structure is an imperfection. An elementary atomic point defect found in GaAs is the interstitial which occurs when an atom is placed in the interstitial void within the crystal. The energy of formation of an interstitial defect is relatively large for a close-packed crystal structure, but the energy can be relatively small in loosely packed crystal structures such as the diamond and zincblende structures corresponding to the maximum proportion of space which can be filled by the atoms in the lattice structure. Using a hard-sphere model, the maximum proportion of space which can be filled by atoms arranged in the closed-packed crystal structures (i.e., face centered cubic or hexagonal closed-packed) is 0.74 while that in the diamond and zincblende structures is 0.34. Oxygen solute atoms probably fit into the interstices of the solvent GaAs lattice. This explanation is consistent with the observation that a large O 1s peak shifted to a lower BE remains after removal of the Ga- and As-oxides.

The C 1s peak shapes shown in Figure 4.3B are quite complex and change significantly with H atom exposure. Peaks or shoulders due to at least five different carbon species are apparent. The predominant peak at 284.6 eV for all the spectra shown is due to the presence of hydrocarbons. A shoulder present at a BE of 286.0 eV is due to adsorbed alcohols, and a shoulder is present at a BE of 287.8 eV due to adsorbed species such as Me_2CO. On the high BE side, a very small shoulder at 289.4 eV may be attributed to the presence of bicarbonate or an organic acid (45). Carbonate species can form at the surface by adsorption of CO_2 from air. The shoulder on the low-BE side at 283.2 eV is most likely due to the presence of Ga carbide (56). Carbon has a relatively small sensitivity factor so the C 1s peak heights in Figure 1a indicate that relatively large amounts of C are present at this surface. As observed in the previous study (56), sputtering/annealing treatments result in the conversion of hydrocarbons to carbide which becomes the

predominant form of C present. This conversion is detrimental because carbide is very difficult to remove. In Figure 4.3B the carbide contribution also is reduced by exposure to H atoms but not as rapidly as the hydrocarbon contribution. Therefore, exposure to hydrogen atoms provides a facile and nondestructive method for removing carbon contamination from GaAs surfaces.

The Ga(LMM) Auger peaks shown in Figure 4.1 are also changed significantly after H-atom exposures. The intensities of the $Ga(L_3M_{4,5}M_{4,5})$ and $Ga(L_3M_{2,3}M_{4,5})$ features at BEs of approximately 190 and 282 eV (KEs of 1063.6 and 971.6 eV respectively) are increased with exposure. High-resolution XPS spectra shown in Figure 4.3B clearly illustrate the enhanced $Ga(L_3M_{2,3}M_{4,5})$ contribution in the C 1s BE region.

Surface chemical processes such as film growth and cleaning occur at the outermost atomic layer even though the migration of species participating in the process alter the subsurface regions. The ISS is a highly surface sensitive analytical tool essentially yielding compositional information about the outermost atomic layer of a solid. Generally, XPS probes more than 30 atomic layers beneath the surface with an exponential fall-off of the electron signal with depth. Typically, less than 10% of the total signal originates from the outermost atomic layer. This information from the outermost atomic layer usually cannot be separated from the subsurface layer information so ISS provides very important, complementary information to XPS data. The principle features in ISS are due to elastic scattering of inert-gas ions (usually He^+ or Ne^+) off atoms at the solid surface.

The ISS spectra obtained from the as-received, solvent cleaned surface using 1-keV He^+ before and after a 15-min, H-atom flux exposure are shown in Figure 4.4Aa and 4.4Ab respectively. The ISS peaks due to C, O, Na, Cl, Ga and As are apparent at E/E_0 values of 0.27, 0.41, 0.54, 0.68 and 0.80 respectively for the scattering angle used in this study. Carbon has a low mass and a high neutralization probability so it is often not detected or yields small features. The small feature in Figure 4.4Aa at an E/E_0 of 0.27 is due to the presence of C. No distinct feature attributable to C is apparent in Figure 4.4Ab.

The As and Ga peaks cannot be resolved using He^+ as the primary ion. The small F peak at an E/E_0 of 0.46 on the *H*-exposed spectrum in Figure 4.4Ab is due to a breakdown of the MACOR® insulation material used in construction of the prototype *H*-atom source at high temperatures. The increased O peak size after *H* atom exposure is due to migration of subsurface O to the surface under a chemical induced driving force. Such an enrichment of the very near surface region in O during reduction has been observed previously during the reduction of TiO_2(001) (61). In these cases a reductive treatment actually enriches the near surface region in O according to ISS.

The ISS spectra obtained from the as-received, solvent-cleaned surface before and after a 15-min, *H*-atom flux exposure using 1-keV Ne^+ are shown in Figure 4.4Ba and 4.4Bb respectively. In this case ISS peaks due to the Ga and As are resolved and appear at E/E_0 values of 0.340 and 0.365 respectively for the scattering angle used in this study. These ISS data indicate that a significantly higher Ga-to-As atom ratio is present on the solvent-cleaned surface compared to the *H* atom exposed surface. This may be due to enrichment of the outermost atomic layer in As during the reductive treatment or preferential coverage of the Ga with O. These Ne^+ ISS spectra are in good agreement with those obtained by Röhkel and Hartnagel (48) and with those presented in the previous study (56) before and after cleaning a GaAs(001) surface by ion sputtering.

Summary

X-ray photoelectron spectroscopy and ISS have been used to examine the near-surface region and outermost atomic layer of polished, air-exposed, solvent-cleaned, n-type (S_i, ~ 3×10^{18} cm^{-3}), GaAs(001) substrates before and after room-temperature exposures to the flux produced by a novel ESD hyperthermal *H*-atom source. The native oxide layer on the solvent-cleaned GaAs(001) substrate contains C, As_2O_5, As_2O_3 and Ga_2O_3 with considerably more Ga oxide than As oxide according to the XPS data. Several forms of C are present including hydrocarbons, alcohols, carbonates and carbide with hydrocarbons as

the predominant species. Upon exposure to the hyperthermal H atom flux, the As oxides are removed more rapidly than Ga oxide, which is consistent with the fact that less As oxide is initially present assuming that they are reduced at similar rates. The C present is removed during the H atom exposure probably by formation and desorption of methane. Most importantly, hydrocarbons are not converted to carbide as in the case with cleaning by ion sputtering. Thus, low-temperature removal of both O and C is possible using this H-atom source. After H-atom treatment, the predominant form of O apparently is a subsurface dissolved or interstitial species according to the XPS data. This is not the case for an ion-sputtered GaAs(001) surface where the predominant O species after nearly complete removal of the O by ion sputtering is a chemisorbed species, which is probably formed by sputter-induced decomposition of the oxides. According to the He^+ ISS data obtained from the solvent-cleaned surface before and after a 15-min. H-atom exposure, the subsurface O migrates to the outermost atomic layer after significant reduction of the Ga- and As-oxides. The Ga-to-As surface atom ratio is decreased for the H-atom exposed surface, and the ratio is similar to that obtained from sputter-etched surfaces. This change may be due to preferential migration of the As to the outermost atomic layer or preferential coverage of the Ga of O which becomes enriched in the very near-surface region by a chemically induced driving potential produced by the H-atoms flux.

Table 4 1 XPS Reference Binding Energies

	Ga 3d	As 3d	O 1s
GaAs	19 4 (62)	41 (62)	—
Ga_2O_3	20.5 (63)	—	530.8 (57)
As_2O_3	—	44.7 (64)	531.6 (62)
As_2O_5	—	46.5 (65)	531.8 (67)
Ga^0	18.6 (57)	—	—
As^0	—	41.5 (66)	—

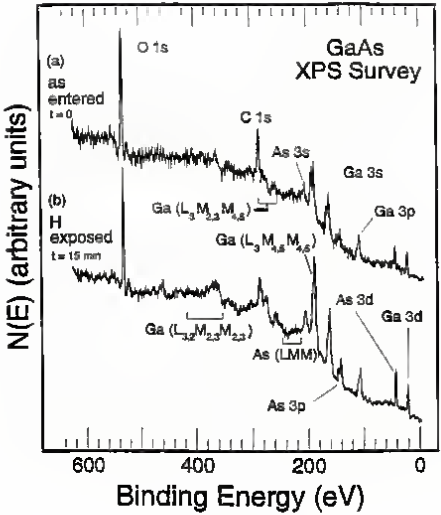

Figure 4.1. XPS survey spectra obtained from a solvent cleaned GaAs(001) surface (a) after insertion into the vacuum system and (b) after a 15 min, room temperature exposure to the hyperthermal H atom flux. Features labeled pertain to both (a) and (b), and the two spectra have been arbitrarily scaled with respect to each other.

The Ga(LMM) Auger peaks shown in Figure 4 1 are also changed significantly after H-atom exposures The intensities of the $Ga(L_3M_{45}M_{45})$ and $Ga(L_2M_{45}M_{45})$ features at BEs of approximately 190 and 282 eV (KEs of 1063 6 and 971 6 eV respectively) are increased with exposure High-resolution XPS spectra shown in Figure 4.3B clearly illustrate the enhanced $Ga(L_3M_{45}M_{45})$ contribution in the C 1s BE region.

Surface chemical processes such as film growth and cleaning occur at the outermost atomic layer even though the migration of species participating in the process alter the subsurface regions. The ISS is a highly surface sensitive analytical tool essentially yielding compositional information about the outermost atomic layer of a solid. Generally, XPS probes more than 30 atomic layers beneath the surface with an exponential fall-off of the electron signal with depth Typically, less than 10% of the total signal originates from the outermost atomic layer. This information from the outermost atomic layer usually cannot be separated from the subsurface layer information so ISS provides very important, complementary information to XPS data. The principle features in ISS are due to elastic scattering of inert-gas ions (usually He^+ or Ne^+) off atoms at the solid surface.

The ISS spectra obtained from the as-received, solvent cleaned surface using 1-keV He before and after a 15-min, H-atom flux exposure are shown in Figure 4 4Aa and 4 4Ab respectively The ISS peaks due to C, O, Na, Cl, Ga and As are apparent at E/E_0 values of 0.27, 0 41, 0 54, 0 68 and 0 80 respectively for the scattering angle used in this study Carbon has a low mass and a high neutralization probability so it is often not detected or yields small features. The small feature in Figure 4 4Aa at an E/E_0 of

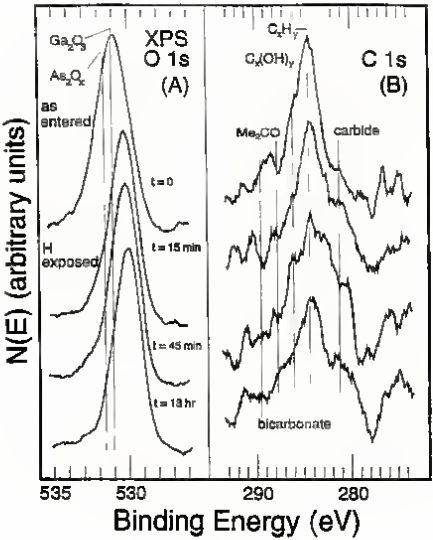

Figure 4.3 XPS (A) O 1s and (B) C 1s spectra obtained from the solvent cleaned. GaAs(001) surface (a) after insertion into the vacuum system and after (b) a 15 min, (c) a 45 min and (d) a 18 h exposure to the hyperthermal H atom flux.

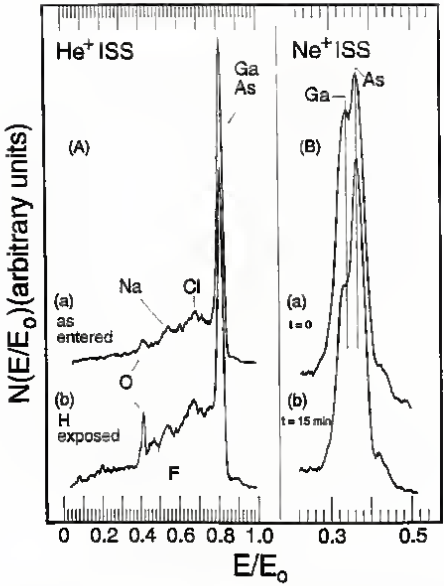

Figure 4.4 ISS spectra obtained from the solvent cleaned, GaAs(001) surface (a) before and (b) after a 15 min room temperature exposure to the 1 eV hyperthermal H-atom flux. The spectra in (A) were obtained using a 1-keV He^+ primary flux, and the spectra in (B) were obtained using a 1 keV Ne^+ primary flux.

CHAPTER 5
CHEMICAL ALTERATIONS OF THE NATIVE OXIDE LAYER ON InP(111) BY THE EXPOSURES TO HYPERTHERMAL ATOMIC HYDROGEN

Recently, *in-situ* cleaning by exposing InP surfaces to H_2 plasmas generated by ECR, microwave (MW) or rf generators has been shown to be effective in removing the native oxide and also in passivating the surfaces by blocking the electrical activity of dangling and defective bonds with H (68-72). However, these sources are expensive and physically incompatible with standard MBE equipment. They operate at high pressures and produce large amounts of contamination and ions. Furthermore, a direct and prolonged exposure to H_2 plasmas can preferentially remove phosphorus, leaving a metallic indium-rich surface (10,73) and can induce surface roughening with loss of the mirror-like aspect.

Thus far, most of the InP studies have focused on the (100) and (110) surfaces with only a few studies on the (111) surface (19,74-77). This may be due to the difficulties encountered in obtaining a clean mirror finish on this surface using conventional procedures (75)

A surface characterization study using XPS and ISS has been performed on polished, solvent-cleaned, undoped InP(111) substrates before and after room-temperature exposure to the flux produced by a novel atomic hydrogen source based on ESD of hyperthermal (~ 1 eV) hydrogen atoms The native oxide layer on the solvent-cleaned InP(111) substrate is nonhomogeneous and contains primarily C, O and In and very little P. Indium is present in the near-surface region as $InPO_3$ or $In(PO_3)_3$, crystalline and amorphous InP, and a relatively small amount of In_2O_3 in the subsurface region. Before H-atom exposure the C is present as hydrocarbons, alcohols, carbonates and carbide with hydrocarbons as the predominant chemical state. During room-temperature exposure to the 1-eV hyperthermal H atom flux for 90 min, removal of oxygen and carbon-contamination

occurs with the C content decreasing by 93%. The In:P ratio is initially 2.28 indicative of an In-rich near surface region. After a 15-min and then 90-min H atom exposure, the In:P ratio decreases to 1.30 and 1.11, respectively. According to ISS data, the H atom flux is very effective in removing contamination at the outermost atomic layer which is crucial for epitaxial growth of device-quality thin films.

Experimental

An as-received, polished Sumitomo Industries, Ltd., undoped InP(111) substrate was ultrasonically solvent cleaned in toluene, acetone, trichloroethylene, acetone and ethanol (in that order) and then inserted into an UHV chamber (base pressure < 10^{-10} Torr). X-ray photoelectron spectroscopy and ISS were performed using a double-pass CMA (PHI model 25-270AR). The details of the characterization experiments have been described in chapter two.

Results and Discussion

The XPS survey spectra obtained from an as-received, solvent-cleaned InP(111) surface before and after a 15- and then 90-min, H atom exposure are shown in Figure 5.1a, b and c, respectively. Peak assignments shown in Figure 5.1 pertain to all three spectra. The peaks apparent in these spectra include the In core-level and Auger peaks, the P 2s and 2p peaks, the O 1s and Auger peaks, the C 1s peak, the valence band and a small doublet at about 230 eV from the Ta support wire which attached the sample to the sample holder. Transition metal sensitivity factors are relatively large so any contributions from the tantalum wire to the O or C features can be neglected. Significant changes in peak shapes, positions and relative peak heights are observed for the In, P, C and O features due to the H-atom exposures. An estimate of the near-surface composition can be obtained from the peak heights in the survey spectra by assuming that this region is homogeneous and using published atomic sensitivity factors (45). The compositions determined in this

manner are presented in table 5.1 for the as-entered, 15- and 90-min exposures to the H atom flux. Both the compositions and the In:P ratios vary considerably with exposure to the H-atom flux. The solvent cleaned sample contains the least In+P (or the most C+O) with the H-atom treated samples containing 67 and 188 at% more In+P for the 15- and 90-min H-atom exposures respectively. For the as-entered sample, the C and O features are large. Both the C and O concentrations decrease with exposure time with the C content decreasing by 93% of its original concentration. The In:P ratio is initially 2.28 indicative of an In-rich, near-surface region. After a 15-min and then a 90-min H-atom exposure, the In:P ratio decreases to 1.30 and 1.11, respectively.

High-resolution XPS P 2p, O 1s, C 1s, In 3d and In Auger spectra obtained from an as received, solvent-cleaned InP(111) substrate before and after exposure to the H-atom flux for 15- and 90-min periods are shown in Figures 5.2 through 5.4. Significant variations in peak shapes and positions are observed between nonexposed and exposed surfaces, indicating that the nature of the chemical species present is altered significantly by exposure to the H-atom flux. X-ray photoelectron spectroscopy has been used to examine species present at native oxide surfaces on InP in numerous studies. Generally, the XPS spectra obtained from these surfaces are complex because many different compounds are present. Unfortunately, the spectral resolution often is not high enough to resolve closely spaced peaks, and the interpretation of the absolute binding energy (BE) values for the unambiguous assignment of the indium and phosphorus environments can be complicated by the surface Fermi level pinning energy and structural modifications such as relaxation (48,78). This is particularly true in the identification of In species using 3d assignments since all the different chemical states of In considered in this study lie within a narrow BE range. However, phosphorus in InP (BE = 128.8 eV) can easily be distinguished from oxidized phosphorus compounds (BE @ 132-135 eV). For these oxides, however, it is difficult to ascertain the relative amounts of various compounds such as $InPO_4$ (BE = 134.0 ± 0.2 eV), $InPO_3$ (BE = 133.5 ± 0.2 eV) and $In(PO_3)_3$ (BE = 133.7 ± 0.2 eV) from

the shape of the P 2p peak. The reference BE values for the indium and phosphorus compounds have been discussed previously (33) and are reported in table 5.2.

The P 2p peaks shown in Figure 5.2 indicate that phosphorus is present as InP, elemental phosphorus In phosphates, and P_2O_5 A significant amount of elemental phosphorus is present on all three surfaces. The predominant P 2p peak lies at 128.8 eV and is assigned as crystalline InP (79). A peak from an unidentified phosphorus species lies at about 127.8 eV which is consistent with that observed by Hoekje and Hoflund (33). The phosphorus peak shapes obtained from the unexposed and H atom exposed surfaces exhibit a shoulder at a P 2p BE of about 129.3 eV assigned in this study to amorphous InP (a-InP) (80). This peak is in agreement with that observed by Hoekje and Hoflund (33), but no assignment was made in that study. With increasing H-atom exposure, the amorphous portion of the predominant peak becomes more enhanced. This fact suggests that the InP which forms under the H atom treatment is amorphous. The feature assigned as InP_xO_4 (consisting of $InPO_4$, $In(PO_3)_3$ and $InPO_3$) varies with regard to both shape and intensity. It primarily broadens to lower BE as phosphate is converted to hiphosphate by chemical reaction with the atomic H. Another feature is present at a BE of about 135.6 eV in (a) due to P_2O_5. This feature is eliminated by the H atom exposure. Since the chemical changes possible are many and complex, only limited information can be deduced from these spectra. The P_2O_5 may be converted to a phosphate, a hiphosphate or elemental phosphorus by the H-atom flux.

The XPS O 1s features obtained from the sample are shown in Figure 5.3A before and after the incremental-time exposures to the H-atom flux. Many different chemical states of oxygen are present on these surfaces, and they all contribute to the O 1s feature. Peaks and shoulders due to In_2O_3, $InPO_4$, $In(PO_3)_3$, $In(OH)_3$, P_2O_5, and H_2O species are present as well as an unidentified feature at 531.2 eV. All of these features including the unknown predominant species were observed by Hoekje and Hoflund (33). In (a) the predominant In species are $InPO_4$ and $In(PO_3)_3$ which makes this feature broad. A

smaller prominent shoulder due to In_2O_3 is also present. The shoulder on the high BE side is due mostly to P_2O_5 since a large peak due to P_2O_5 is present in the P 2p spectrum. A small peak due to nonbridging P_2O_5 (79) is also present. With increasing exposure the predominant peak develops a more symmetrical shape and shifts toward lower BE indicating that chemical changes occur during the H-atom exposures. As shown in table 5.2, the oxygen content of the near surface region is significantly reduced by the H-atom flux. The shoulder due to In_2O_3 is reduced, which is consistent with the In 3d spectra discussed below. Based on the P 2p spectrum, the P_2O_5 is eliminated by H-atom exposures so the broadened shoulders in (b) and (e) are due to enhanced OH^- signals. According to the P 2p spectra, the H-atom exposure converts $InPO_4$ and $In(PO_3)_3$ to biphosphates. Therefore, the narrowing of the O 1s feature and the increased prominence of the 531.2-eV feature imply that this peak is due to In biphosphate. These data suggest that In biphosphate is less susceptible to decomposition by H-atoms than other In and P species present, which is reasonable since the biphosphate forms through reactions induced by the H-atoms. In (c) the shoulder due to In_2O_3 is diminished further, the $In(OH)_3$ shoulder is enhanced and only a fairly well-defined peak due to In biphosphate is present. The decomposition of the In phosphates may occur through conversion to In biphosphates initially and then to $In(OH)_3$.

The C 1s peak shapes shown in Figure 5.3B significantly with H-atom exposure. Peaks or shoulders due to the presence of several different carbon species are apparent. The predominant peak at 284.6 eV for all the spectra shown is due to hydrocarbons, and a shoulder present at a BE of about 286.0 eV is due to adsorbed alcohols. The shoulder on the low BE side at about 282.7 eV most likely is due to the presence of a carbide since carbides have C 1s BEs below 283.0 and other C-containing compounds have higher BEs. Neither In carbide nor P carbide are known to exist as bulk compounds. However, III carbides such as Al_4C_3 are known to exist (80) whereas V carbides apparently have not been synthesized or identified previously. Based on these facts the low-BE feature

observed in this study is assigned as In carbide. An estimate of the near-surface composition using the homogeneous assumption gives an initial carbon content of 42.1 at% which is reduced to only 3.0 at% after the 90-min H-atom exposure. Therefore, exposure to hydrogen atoms provides a facile method for removing carbon contamination from InP surfaces.

The In 3d peaks shown in Figure 5.4A are fairly narrow and well-defined even though multiple In chemical states contribute to these features. These peaks do change in a subtle manner with increasing H-atom exposure. They become more narrow, and the peak maximum shifts a few tenths of an eV from that of In_2O_3 to InP. The known presence of In_2O_3, $InPO_4$, $In(PO_3)_3$ and $In(OH)_3$ broaden the InP feature to the high-BE side according to the data in table 5.2. For these species the O-to-In ratios are 1.5, 4, 9 and 3, respectively. Based on these O-to-In ratios, the O concentrations in table 5.1, and the information provided by the O 1s features, only a fairly small fraction of the In is bonded as In_2O_3, $InPO_4$, $In(PO_3)_3$, $In(OH)_3$ and In biphosphates. This explains why the peaks in Figure 5.4A are broadened to the high BE side and an distinct shoulder due to these species is present. The In $3d_{5/2}$ spectra shown in Figure 5.4B of the study by Hoffund and Corallo (32) are consistent with this explanation. Studies often focus on the In 3d features for chemical state evaluation even though information is difficult to obtain since the chemical shifts are small. High-resolution Auger spectra for the dominant In peaks at a kinetic energy of about 400.9 eV (BE = 852.7 eV) are shown in Figure 5.4B. The Auger spectra obtained from the solvent-cleaned InP(111) surface before and after 15-min and 90-min exposures to the H-atom flux are shown in Figures 5.4Ba, b and c, respectively. The spectra shown in d and e were obtained from a clean InP surface and from an air-cleaned InP surface respectively (81). With increasing H-atom exposure, the spectra become more similar to that obtained from clean InP in that the shoulders on the high-BE side are reduced in size and the peak widths are decreased. The kinetic energy of the $M_5N_{4,5}N_{4,5}$ transition is 403.0 eV (BE = 850.6 eV) which is about 2.0 eV smaller than values reported for In

metal (45 82). This value is also about 0 6 eV larger than values reported for In_2O_3 (82) and agrees with values reported by Clark et al. (83) and Hoflund and Corallo (32) for InP. The air cleaned sample exhibits the opposite effect in that the peak is broader and contains a shoulder on the high-BE side compared to that from clean InP. Compared with the In $3d_{5/2}$ spectra, differences in the In(MNN) features are greater and therefore provide more readily observable chemical state information.

The ISS spectra obtained from the solvent-cleaned InP(111) surface using 1 keV He^+ before and after the H atom flux exposures are shown in Figure 5.5. The change in surface composition of the outermost atomic layer before and after exposure is quite significant. ISS peaks due to C, O, P and In are apparent at E/E_0 values of 0.27, 0.39, 0.62 and 0 88, respectively for the scattering angle used in this study. The large, broad background feature in Figure 5.5a is due to the presence of C and O and is typical of a contaminated, air-exposed surface. This feature is absent after the surface was exposed to the H-atom flux for only 15 min demonstrating the high chemical reactivity of the H-atoms. A large In peak at an E/E_0 of 0 88 is apparent in Figure 5 5b and c after the H-atom exposures, and these spectra are similar to those obtained from a clean InP surface (33) Phosphorus has a lower mass than In and therefore a lower sensitivity factor. Nevertheless, the spectra shown in Figure 5.5b and c indicate that the outermost atomic layers of these surfaces consist mostly of In and O. The spectrum shown in c has a reduced background particularly in the lower E/E_0 region which is consistent with the fact that much more C is removed during the longer H-atom exposure. Although the H-atoms are highly reactive, the cleaning process is slowed by diffusion of subsurface O and C to the outermost atomic layer of the surface where they rapidly react with the atomic H and leave the surface. Heating the sample at fairly low temperatures should increase the rate of cleaning considerably, and it may be possible to produce clean InP surfaces by this method in short periods of time.

Summary

X-ray photoelectron spectroscopy and ISS have been used to examine the near-surface region and outermost atomic layer of polished, air-exposed, solvent-cleaned, undoped InP(111) substrates before and after room-temperature exposures to the flux produced by a novel ESD hyperthermal H atom source. The native oxide layer on the solvent-cleaned InP(111) substrate is nonhomogeneous and contains primarily C, O and In and very little P. Indium is present in the near-surface region as $InPO_4$ or $In(PO_3)_3$, c-InP and a-InP, and a small amount of In_2O_3. Several forms of C are present including hydrocarbons, alcohols, and carbide with hydrocarbons as the predominant species. Upon exposure to the hyperthermal H-atom flux, low-temperature removal of oxygen and carbon contaminants occurs, and the near-surface region appears to approach the stoichiometry of a clean InP(111) surface. The In:P ratio decreases from an initial value of 2.28 for the solvent-cleaned sample to 1:1. According to the He^+ ISS data, the H-atom flux is very effective in removing contamination near the surface, and then diffusion of subsurface O to the outermost atomic layer becomes the rate-controlling step.

Table 5.1. Compositions Determined from XPS Data Obtained from Solvent Cleaned and H Atom Exposed InP(111) Surfaces

Substrate Treatment	Composition (at%)					
	P	C	In	O	In+P	In/P
Solvent cleaned	7.8	42.1	17.8	32.3	25.6	2.28
after 15 min H atom exposure	18.6	27.5	24.2	29.7	42.8	1.30
after 90 min H-atom exposure	35.0	3.0	38.8	23.2	73.8	1.11

Table 5.2. XPS Binding Energies Used to Evaluate Chemical States

Compound	BE Peak Position (eV)			
	In $3d_{5/2}$	In 4d	P 2p	O 1s
a-InP (44)	444.3	17.8	129.25	—
c-InP	444.5	18.6	128.8	—
In	443.6	16.4	—	—
P	—	—	130.2	—
In_2O_3	444.6	—	—	530.2
$In(OH)_3$	445.2	—	—	531.8
$InPO_4$	445.6	—	134.0	531.8
$In(PO_3)_3$	445.4	—	133.7	531.5
P_2O_5	—	—	135.6	532.7
P_4O_{10}	—	—	135.5	531.7

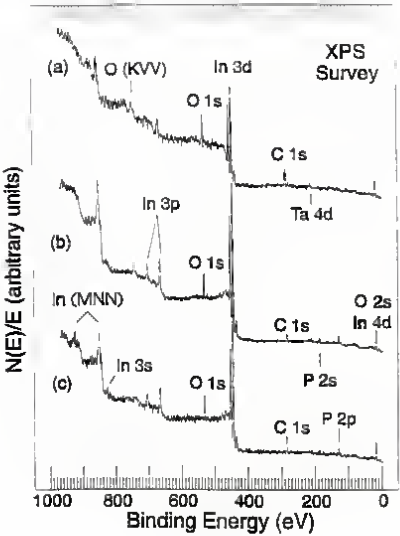

Figure 5.1. XPS survey spectra obtained from a solvent cleaned InP(111) surface (a) after insertion into the vacuum system, (b) after a 15-min and (c) after a 90 min, room-temperature exposure to the hyperthermal H-atom flux. Features labeled pertain to all three spectra, and the three spectra have been arbitrarily scaled with respect to one another.

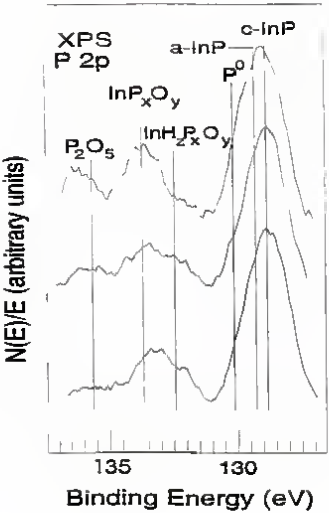

Figure 5.2. XPS P 2p spectra obtained from the solvent-cleaned, InP(111) surface (a) after insertion into the vacuum system, (b) after a 15 min and (c) 90 min exposure to the hyperthermal H atom flux.

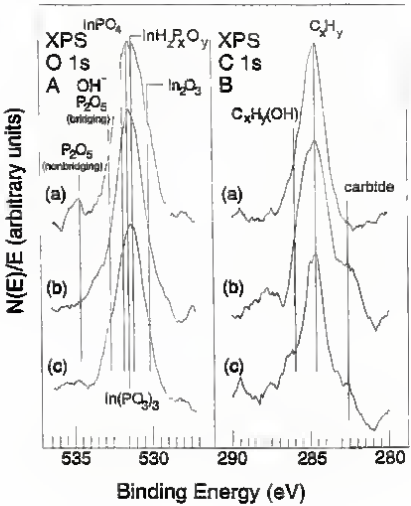

Figure 5.3 XPS (A) O 1s and (B) C 1s spectra obtained from the solvent-cleaned InP(111) surface (a) after insertion into the vacuum system, (b) after a 15 min and (c) 90 min exposure to the hyperthermal H-atom flux.

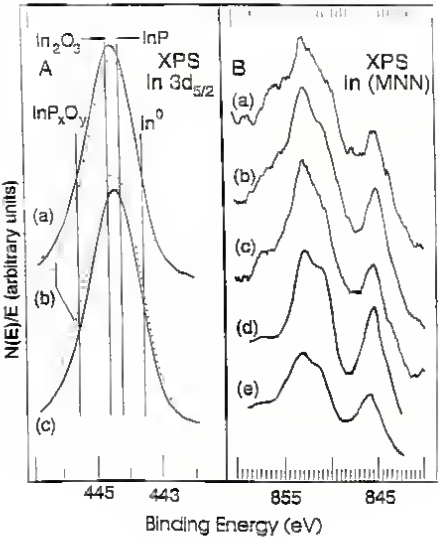

Figure 5.4 (A) XPS In $3d_{5/2}$ spectra and (B) XPS In(MNN) Auger spectra obtained from the solvent-cleaned, InP(111) surface (a) after insertion into the vacuum system, (b) after a 15 min and (c) 90 min exposure to the hyperthermal H atom flux. In (B) (d) was obtained from a clean InP surface and (e) was obtained immediately after cleaving an InP sample in air

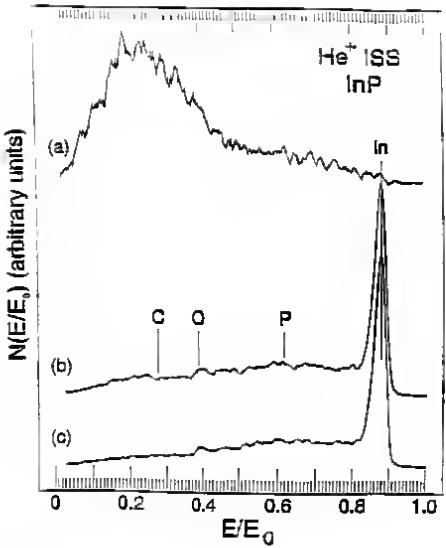

Figure 5.5 ISS spectra obtained using a 1-keV He^+ primary flux from the solvent cleaned InP(111) surface (a) before, (b) after 15 min and (c) 90 min room temperature exposures to the 1 eV hyperthermal H-atom flux.

CHAPTER 6
ROOM TEMPERATURE OXIDATION OF A GaAs(001) SURFACE INDUCED BY THE INTERACTION OF HYPERTHERMAL ATOMIC OXYGEN STUDIED BY XPS AND ISS

In this study a novel hyperthermal oxygen atom source has been used to form an oxide layer on an Ar^+ sputtered GaAs(001) surface at room temperature, and this layer has been examined using XPS and ISS. The XPS data indicate that the Ga in the near-surface region is oxidized predominantly to Ga_2O_3 with a significant contribution from $GaAsO_4$ while the As is oxidized predominantly to an AsO_x species with significant contributions from As_2O_3 and $GaAsO_4$ and/or As_2O_5. The oxide layer thickness is estimated to be about 25 Å, and the XPS Ga:As atom ratio increases from 1:1 to 1:6 during the oxidation. The ISS data indicate that the resulting oxide layer formed is more electrically insulating than a native oxide layer on this surface.

Experimental

An as-received, Sumitomo Industries Ltd., Si-doped n-type GaAs(001) substrate with a carrier concentration of approximately 3×10^{18} cm^{-3} was ultrasonically solvent cleaned in toluene, acetone, trichloroethylene, acetone and ethanol (in that order). To duplicate typical ex-situ substrate preparation, removal of the air-exposed oxide layer and surface contaminants, such as carbon the solvent-cleaned sample was wet etched for 30 s in a 7:1:1 solution of H_2SO_4:H_2O_2:H_2O rinsed with DI water for 5 min then placed in concentrated HCl for 5 min followed by a 5 min DI water rinse. The sample was then inserted into an UHV chamber (base pressure < 10^{-10} Torr) as quickly as possible to minimize air exposure to the prepared surface. X-ray photoelectron spectroscopy and ISS data were first obtained from the as-entered sample. The surfaces next were sputtered with

1-keV Ar^+ for 15 min to further reduce the O and C contaminants from the surface and near surface regions as observed in XPS survey spectra. The sample was transferred into an adjoining UHV chamber which houses the atom source via a magnetically coupled rotary/linear manipulator. The surface was then exposed to the hyperthermal O flux and re-examined after a total exposure time of 15 hrs. The sample was not examined at intermittent time intervals so the rate of oxidation as a function of time has not been determined in this study. The effect of sample temperature also has not been examined, and this variable is most likely quite important with regard to the diffusion rate of Ga and As atoms to the surface where they react with the atomic O.

Results and Discussion

The XPS survey spectra obtained from the Ar^+-sputtered GaAs(001) surface described above before and after the 15 hr O-atom exposure are shown in Figure 6.1a and b respectively. Peak assignments shown in Figure 6.1 pertain to both spectra. Significant changes in peak shapes, positions and relative peak heights are observed for Ga, As and O. An estimate of the near-surface composition can be obtained from the peak areas in the spectra by assuming that this region is homogeneous and using atomic sensitivity factors (45). The results of such an analysis must be considered semi-quantitative since elemental distributions (geometrical or matrix effects) can have a large influence (84) on the calculated values. The compositions determined in this manner are presented in table 6.1 for the Ar^+-sputtered and 15-hr O-exposed surfaces. Both the composition and the Ga:As ratio vary considerably with exposure to the O-atom flux. In addition to Ga and As, the initial near-surface region contains a relatively small amount of O which was not removed by the Ar^+ sputtering process used. The O concentration greatly increases with O-atom exposure exhibiting approximately a 10-fold increase. The Ga:As ratio is initially 1.1, which is close to that of stoichiometric GaAs. After the 15 h O-atom exposure, the Ga:As ratio is 1.6 due to migration of Ga to the near-surface region. These values are consistent with those found

in previous studies and a proposed oxidation model of both GaAs and InP surfaces examined in this laboratory. Using modified equations proposed by Carlson and McGuire (85), this oxide layer thickness is estimated to be about 25 Å. The modified equations used and assumptions made are presented in Appendix B.

High-resolution XPS As 3d, Ga 3d, O 1s, As 3s and $Ga(L_3M_{4,5}M_{4,5})$ spectra obtained from the solvent cleaned, chemically-etched and 1-keV He^+ ion-etched GaAs(001) substrate (a) before and (b) after the 15 h O-atom exposure are shown in Figures 6.2 and 6.3. Significant variations in peak shapes and positions are observed between nonexposed and O-exposed surfaces in all sets of spectra indicating that the nature of the chemical species present is altered significantly by exposure to the O-atom flux. The As and Ga 3d peaks shown in Figure 6.2a indicate that As_2O_3 and As_2O_5 are not initially present, an As^0-rich region lies above the bulk GaAs (56), a small amount of AsO_x (a suboxide) may also be present, and a small Ga_2O_3 contribution is apparent as a shoulder on the high-BE side of the Ga 3d peak. After exposure to the O-atom flux, As_2O_3, As_2O_5, Ga_2O_3 and $GaAsO_4$ are all present in the near-surface region according to the XPS spectrum shown in Figure 6.2b. Furthermore, the predominant As 3d feature is shifted to a higher BE of 42.5 eV which is assigned as a suboxide of As probably As_2O (86).

The O 1s peak shapes and positions obtained from the surface before and after exposure to the O-atom treatment are shown in Figure 6.3Aa and b. Initially, Ga_2O_3 is the predominant oxide species, and structure due to As_2O_3 or As_2O_5 is not apparent, which is consistent with the data shown in Figure 6.2a. After exposure to O the O 1s peak increases in height, develops a more symmetrical shape and shifts toward higher BE. These observations are consistent with the increase in As oxides as observed in the As 3d spectra of Figure 6.2b. Although the predominant O 1s feature has a BE which coincides with these of As_2O_3 and As_2O_5 this feature is due to O in the As suboxide as discussed above. A distinct shoulder due to Ga_2O_3 is present on the low-BE side of this feature. A very small shoulder is present on the high-BE side due to the presence of surface water. This

water either adsorbs on the oxide surface from the residual gas in the UHV chamber or forms by reaction of the background H_2 with surface oxygen. The As 3s and $Ga(L_3M_{4,5}M_{4,5})$ features shown in Figure 6.3B also exhibit interesting changes due to oxidation. The As 3s peak is reduced in height and broadened due to formation of As oxides. The $Ga(L_3M_{4,5}M_{4,5})$ peak is split into two peaks and broadened. The higher BE peak is due to Ga oxide formation. This Auger feature is more sensitive to oxidation than the Ga 3d feature. The As 3s feature is reduced in intensity by oxidation because the near-surface region becomes enriched in both Ga and O.

A 1-keV He^+ ISS spectrum obtained from the Ar^+-sputtered GaAs(001) surface is shown in Figure 6.4a. It contains features due to O, Ga and As at E/E_0 values of 0.39, 0.79 and 0.81, respectively. The Ga and As features are so closely spaced that they cannot be resolved using He^+. A small Si feature at about the noise level appears to be present at an E/E_0 of 0.63. This Si feature results from the Si doping. In ISS the sensitivity increases with mass so even though the O feature is small the amount of O in the outermost atomic layer is not negligible. The background in ISS spectra consists of ions which scatter multiple times and then leave the surface as ions. The height of the background provides a measure of the electrical conductivity of the surface, i.e., as the conductivity increases the background decreases due to enhanced neutralization of the ions (87). Spectra obtained from the O atom-exposed GaAs(001) surface and the native oxide layer on the GaAs(001) surface are shown in Figure 6.4b and c, respectively. Very small Si and Ga/As features are observed in spectrum b. The large feature is a charging peak which is also characteristic of highly insulating surfaces (88). By comparison the ISS spectrum obtained from the native oxide layer has a large background characteristic of a surface which is not very conductive, but it does not contain a large charging feature as in Figure 6.4b. These spectra indicate that the oxide layer formed by exposure of the cleaned GaAs(001) is significantly more electrically insulating than the native oxide.

Summary

In this study a novel hyperthermal oxygen atom source has been used to form an oxide layer on an Ar^+ sputtered GaAs(001) surface at room temperature, and this layer has been examined using XPS and ISS. The XPS data indicate that the Ga in the near-surface region is oxidized predominantly to Ga_2O_3 with a significant contribution from $GaAsO_4$ while the As is oxidized predominantly to an AsO_x species with significant contributions from As_2O_3 and $GaAsO_4$ and/or As_2O_5. Using modified equations proposed by Carlson and McGuire, this oxide layer thickness is estimated to be about 25 Å. The XPS Ga:As atom ratio increases from 1.1 to 1.6 during the oxidation. The As 3s peak is reduced in height and broadened due to formation of As oxides. The $Ga(L_3M_{4,5}M_{4,5})$ peak is split into two peaks and broadened. The higher BE peak is due to Ga oxide formation. This Auger feature is more sensitive to oxidation than the Ga 3d feature. The As 3s feature is reduced in intensity by oxidation because the near-surface region becomes enriched in both Ga and O. The ISS data indicate that the resulting oxide layer formed is more electrically insulating than a native oxide layer on this surface.

Table 6.1 Composition Determined from XPS Data Obtained from Solvent Cleaned, Etched/Sputtered and O Atom Exposed GaAs(001) Surfaces

Substrate Treatment	Composition (at%)				
	O	C	Ga	As	Ga:As
Solvent-cleaned, wet etched and Ar^+ sputtered	6.8	3.3	47.1	42.8	1.1
After 15 h O-atom exposure	67.6	0.0	19.8	12.6	1.6

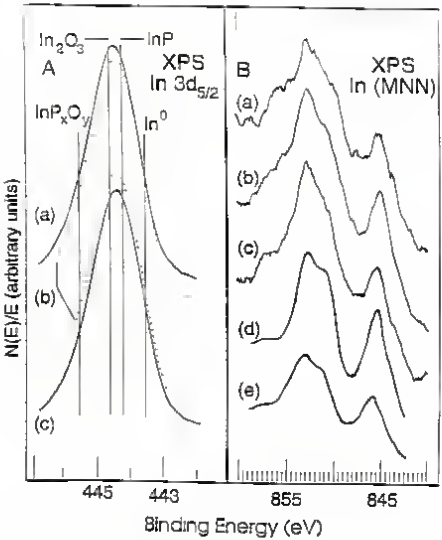

Figure 5.4 (A) XPS In $3d_{5/2}$ spectra and (B) XPS In(MNN) Auger spectra obtained from the solvent-cleaned InP(111) surface (a) after insertion into the vacuum system, (b) after a 15 min and (c) 90 min exposure to the hyperthermal H-atom flux. In (B) (d) was obtained from a clean InP surface and (e) was obtained immediately after cleaving an InP sample in air

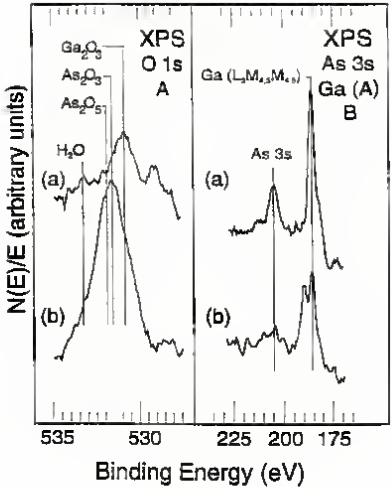

Figure 6.3 XPS (A) O 1s and (B) As 3s and Ga($L_3M_{4,5}M_{4,5}$) spectra obtained from the solvent cleaned, chemical and ion-etched GaAs(001) substrate (a) before and (b) after a 15 h, room temperature exposure to the hyperthermal O atom flux.

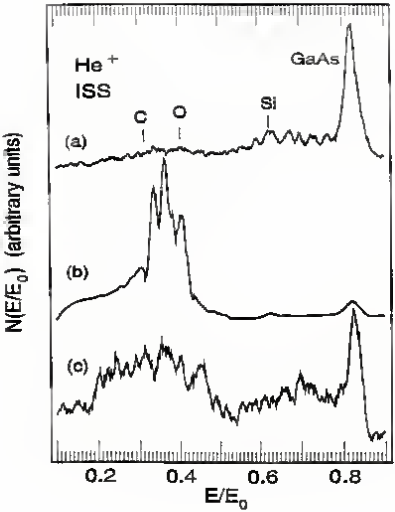

Figure 6.4 He+ ISS spectra obtained from the solvent-cleaned, chemical and ion-etched GaAs(001) substrate (a) before and (b) after a 15 h room-temperature exposure to the hyperthermal O-atom flux. The spectrum shown in (c) was obtained from a native-oxide layer on GaAs(001)

REFERENCES

1. S. M. Sze, Physics of Semiconductor Devices, second edition, Wiley-Interscience publication, John Wiley & Sons, NY 1981

2. J. L. Freeouf, J. A. Silberman, S. L. Wright, S. Tiwari and J. Batey, J. Vac. Sci. Technol. B 7(1989)854

3. L. Sorba, G. Bratina, G. Ceccone, A. Antonini, J. F. Walker, M. Micovic and A. Franciosi, Phys. Rev. B 43(1991)2450

4. P. J. Palomares, M. A. Mendez, M. T. Cuberes and F. Soria, J. Vac. Sci. Technol. A 9(1991)939

5. J. Falta, R. M. Tromp, M. Copel, G. D. Pettit and P. D. Kirchner, Phys. Rev. Lett. 69(1992)3068

6. A. Ichimiya, Q.-K. Xue, T. Hashizume and T. Sakurai, J. Crystal Growth 150(1995)136.

7. C. M. Reuleau and R. M. Park, J. Appl. Phys. 73(1993)4610.

8. N. Kouode and Y. Nanishi, Jpn. J. Appl. Phys., Part 1 28(1989)L7

9. S. V. Hattangady, R. A. Rudder, M. J. Mantini, G. G. Fountain, J. B. Posthill and R. J. Markunas, J. Appl. Phys. 68(1990)1233

10. D. Gallet, G. Hollinger, C. Santinelli and L. Goldstein, J. Vac. Sci. Technol. B 10(1992)1267

11. A. Guivarch, H. L'Haridon, G. Pelous, G. Hollinger and P. Pertosa, J. Appl. Phys. 55(1984)1139

12. M. Losurdo, P. Capezzuto and G. Bruno, J. Vac. Sci. Technol. B 14(1996)691

13. N. J. Kawai, C. E. C. Wood and L. F. Eastman, J. Appl. Phys. 53(1982)6208.

14. A. Takamori, S. Sugata, K. Asakawa, E. Miyauchi and H. Hashimoto, Jpn. J. Appl. Phys. 26(1987)L142.

15. Z. Lu, M. T. Schmidt, D. Chen and R.M. Osgood, Jr., W. M. Holber, D. V. Podlesnik and J. Foster, Appl. Phys. Lett. 58(1991)1143

16. T. Sugaya and M. Kawabe, Jpn. J. Appl. Phys. 30(1991)L402.

17. E.J. Petit, F. Houzay and J. M. Moisson, J. Vac. Sci. Technol. A 10(1992)2172.

18 J Ramm, E. Beck, J Eisele W Hansch B U Kleeser and H Senn Mat. Res Soc Symp Proc 315(1993)91

19 M. Yamada and Y Ide. Jpn. J. Appl. Phys. 33(1994)L671.

20 M. Losurdo, F. Capezzuto and G. Bruno J. Vac Sci. Technol B 14(1996)691

21 Y Okada and J S Harris, Jr., J Vac. Sci. Technol. B 14(1996)1725

22. H. Shimomura, Y Okada and M. Kawabe, Jpn J Appl. Phys 31(1992)L628.

23 T Sugaya, M Kaneko, Y Okada and M Kawebe, Jpn J Appl. Phys 32(1993)L1834

24 H. Shimomura, Y. Okada, H. Matsumoto, M. Kawabe, Y Kizami and Y Bando, Jpn. J. Appl. Phys. 32(1993)632.

25. I. Suemene, Y Kunitsugu, Y Kan and M Yamanishi, Appl. Phys Lett. 55(1989)760

27 Y Okada, S Ohta, A Kawabata and M Kawabe, Jpn J Appl. Phys 32(1993)L1556

28 Y Okada, H. Shimomura and M. Kawabe, J Appl. Phys 73(1993)7376.

29 Y Okada, S Ohta, A Kawabata, H. Shimomura and M. Kawabe, J Elec Mat. 25(1994)331.

30. F. Silva-Andrade, F Chavez and E. Gomez, J Appl. Phys. 76(1994)1946.

31. EPI Application Note, August/September, 1994

32 G.B Hoflund and Cheryl F Corallo, Surf Inter Anal. 9(1986)319

33 S.J Hoekje and G B Hoflund, Thin Solid Films 197(1991)367.

34 S.J. Hoekje and G B Hoflund, Appl. Surface Sci. 47(1991)43.

35 R. A. Outlaw S N Sankaran, G B Hoflund and M R. Davidson, J Mater Res. 3(1988)1378.

36 R. A. Outlaw, G B Hoflund and G R. Corallo, Appl. Surf Sci. 28(1987)235

37 G. B Hoflund, Scan. Elect. Microsc. IV(1985)1391.

38 D. A. Dahl and J E. Delmore, SIMION Computer Software Package, Idaho National Engineering Laboratory (1987)

39 M. R. Davidson, G B Hoflund and R A Outlaw J Vac Sci. Technol. A 11(1993)264

40 M. R. Davidson, G. B Hoflund and R. A. Outlaw Surf Sci. 28(1993)111.

41 C. F. Corallo, D. A. Asbury, M. A. Pipkin, T. J. Anderson and G. B. Hoflund, Thin Solid Films 139(1986)299.

42 R. E. Gilbert, D. F. Cox and B. B. Hoflund, Rev. Sci. Instr. 53(1982)447.

43 A. Savitzky and M. J. E. Golay, Anal. Chem. 36(1984)1627.

44 N. J. Kawai, C. E. C. Wood and L. F. Eastman, J. Appl. Phys. 53(1982)6208.

45 C. D. Wagner, W. M. Riggs, L. E. Davis, J. F. Moulder and G. E. Muilenberg (eds.) Handbook of X ray Photoelectron Spectroscopy, Perkin-Elmer Corporation, Prairie, MN, 1979.

46 S. J. Hoekje, M. R. Davidson and G. B. Hoflund, Chem. Mater. 3(1991)77.

47 G. B. Hoflund and D. M. Minahan, J. Catal. 162(1996)48.

48 K. Röhkei and H.L. Hartnagel, Int. J. Elec. 6(1986)663.

49 C.D. Thurmond, G.P. Schwartz, G.W. Kammlott and B. Schwartz, J. Electrochem. Soc., SolidState Science and Technology 127(1980)1366.

50 H. Niehus, W. Heiland and E. Taglauer, Surface Sci. Reports 17(1993)213.

51 V.Y. Young and G.B. Hoflund, Anal. Chem. 60(1988)269.

52 V.Y. Young, G.B. Hoflund and A.C. Miller, Surface Sci. 235(1990)60.

53 O. Melendez, G.B. Hoflund, R.E. Gilbert and V.Y. Young, Surface Sci. 251/252(1991)228.

54 V.Y. Young, N. Welcome and G.B. Hoflund, Phys. Rev. B 48(1993)2891.

55 H.H. Brongersma and H.J. van Daal, Analysis of Microelectronic Materials and Devices (1991) 389.

56 J. T. Wolan, W. S. Epling and G. B. Hoflund, J. Appl. Phys. 81(1997)6160.

57 O. Schoen, J. Electron Spectrosc. Relat. Phenom. 2(1973)75.

58 J.P. Contour, J. Massies and A. Saletes, Jpn. J. Appl. Phys. 24(1985)L563.

59 J.F. Weaver and G.B. Hoflund, J. Phys. Chem. 98(1994)8519.

60 J.F. Weaver and G.B. Hoflund, Chem. Mater. 6(1994)1693.

61 G.B. Hoflund, H.L. Yin, A.L. Grogan Jr., D.A. Asbury, H. Yooeyama, O. Ikeda and H. Tamura, Langmuir 4(1988)346.

62 J.A. Taylor, J. Vac. Sci. Technol. B 20(1982)751.

63 H. Iwakuro, C. Tatsuyama and S. Ichimura Jpn. J. Appl. Phys. 20(1982)94.

64 P.A. Breeze, H.L.Hartnagel., P.M.A. Sherwood, J. Electrochem. Soc. 127(1980)454

65 W.J. Stec, W.E. Morgan, R.G. Albridge and J.R. Van Wazer, Inorg. Chem. 11(1972)220.

66. E.D. Roberts, P. Weightman and C.E. Johnson, J. Phys. Chem. 8(1975)1301

67. Y. Mizokawa, H. Iwasaki, R. Nishitani and S. Nakamura, J. Electron Spectrosc. Relat. Phenom. 14(1978)129

68 A.J. Nelson, S. Frigo, D. Mancini and R. Rosenberg, J. Appl. Phys 70(1991)5619.

69 P.G. Hofstra, D.A. Thompson, B.J. Robinson and R.W. Streater, J. Vac. Sci. Technol. B 11(1993)985

70 T. Sugino, H. Ninomiya, T. Yamada, J. Shirafuji and K. Matsuda. Appl. Phys. Lett. 60(1992)1226.

71 T. Sugino, H. Yamamoto and J. Shirafuji, Jpn. J. Appl. Phys. 30(1991)L948

72. C.W. Tu, R.P.H. Chang and A.R. Schlier, Appl. Phys. Lett. 41(1982)80.

73. M. Yamaguchi and K. Ando, J. Appl. Phys. 51(1980)5007.

74 P.A. Kohl, C. Wolowodiuk and F.W. Ostermayer, Jr., J. Electrochem. Soc. 130(1983)2288

75. S.N.G. Chu, C.M. Jodlauk and W.D. Johnston, Jr., J. Electrochem. Soc 130(1983)2398

76. Dai Daoxuan and Zhu Furang, Chin. J. Semicond. 6(1985)190

77. J.R. Waldrop, S.P. Kowalczyk and R.W. Grant, Appl. Phys. Lett. 42(1983)454.

78. M. Quchene, C. Senemaud, E. Belin, A. Gheorghiv and M. Theye, J. Non-cryst. Solids 59/60(1983)625

79 J.F. Moulder, W.F. Stickle, P.E. Sobel and K.D. Bomben, Handbook of X-ray Photoelectron Spectroscopy, edited by J. Chastain, Perkin Elmer Corporation, Eden Prairie, MN 1992.

80. R. C. Weast (editor), CRC Handbook of Chemistry and Physics, CRC Press, Inc., Boca Raton 1985.

81. D. M. Poirier and J. H. Weaver, Surface Sci. Spectra 2(1994)256

82. A. C. Parry Jones, P. Weightmann and P. T. Andrews, J. Phys. C. Solid State Phys. 12(1979)1587

83 D. T. Clark, T. Fox, G. G. Roberts and R. W. Sykes, Thin Solid Films 70(1980)261.

84 G.B. Hoflund in Handbook of Surface and Interface Analysis: Methods in Problem Solving, edited by J.C. Riviere and S. Myhra, Marcel Dekker Inc., New York, NY, 1998, p. 57.

85 T.A. Carlson and G.E. McGuire, J. Elect. Spectrosc. Relat. Phenom. 1(1972/73)161.

86 B.J. Flinn and N.S. McIntyre, Surface Inter. Anal. 15(1990)19.

87 S.D. Gardner, G.B. Hoflund, M.R. Davidson and D.R. Schryer, J. Catal. 115(1989)69.

88. S.D. Gardner, G.B. Hoflund, D.R. Schryer and B.T. Upchurch, J. Phys. Chem. 95(1991)835.

89. S. Tanuma, C.J. Powell and D.R. Penn, Surf. Interface Anal. 12(1988)577.

APPENDIX A
ATOMIC OXYGEN FLUX QUANTIFICATION

A clean Pt foil was exposed to an O-atom flux for 1 min and the atom coverage was determined using ion scattering spectroscopy (ISS). After exposure ISS data was taken in 5 minute increments until the Pt signal stabilized to a maximum value for three consecutive readings as shown in the graph below. The change in fractional oxygen coverage was then determined as a function of atomic flux, the oxygen sticking coefficient and a target to source factor. The equations used and assumptions made are present below

$$r = \frac{d\theta}{dt} = FSD(1-\theta)$$

$$\int_0^\theta \frac{d\theta}{(1-\theta)} = \int_0^t FSdt$$

$$-\ln(1-\theta) = FSDt$$

$$F = \frac{1}{SDt}\left[-\ln(1-\theta)\right]$$

where F is the atomic flux, S = the O sticking coefficient for Pt, t = 60 s, D is the correction factor for source to target distance, and θ = the O fractional coverage.

For these results:

$$F = \left(\frac{1}{0.177}\right)\left(\frac{2\times10^{13}}{60s}\right)\left(-\ln(1-\theta)\right)$$

θ	F for 60 sec exposure	q = (8192-2906)/8192 = 0.645
0.1	0.2×10^{14} (atoms/cm^{2}s)	flux = 1.95×10^{14} atoms/cm^{2}s
0.2	0.4×10^{14}	
0.3	0.67×10^{14}	
0.4	0.96×10^{14}	
0.5	1.30×10^{14}	
0.6	1.72×10^{14}	

Assumptions:

1. S = 1 If the sticking coefficient is less than 1.0, then the flux will be larger.
2. The factor D for placing the source 7" away from the sample is 1/0.177 = 5.6. For a point source this is 1/0.2 = 50. We believe the actual value is closer to 10 so we chose a conservative value based on geometrical arguments and data points obtained with a previously used O-atom source that is now in use.
3. 1 O atom covers 1 Pt atom in ISS. Again this is conservative since the area for an O atom is 1.3Å^2 and the area for the Pt atom is 10.5 Å^2. If it requires several O atoms to shield a Pt atom in ISS, then the flux would be greater by this amount.

APPENDIX B
MODIFIED ALGORITHM USED TO CALCULATE THE OXIDE THICKNESS GROWN

The expression for the XPS intensities of an overlayer A of finite thickness on an infinitely thick substrate B are as follows

$$I_A = K_A \lambda_A \sin\theta \left[1 - \exp\left(-\frac{t_A}{\lambda_A}\sin\theta\right)\right]$$

where t_A is the thickness of A, λ_A is the inelastic mean free path (IMFP) of A's photoelectrons in material A, K_A is a term containing the effect of X-ray intensity, photoemission cross-section and analyzer transmission for the photoelectrons of A, θ is the take-off angle relative to the sample surface plane, and, implicitly, $C_A = 1$ (concentration of A).

Similarly

$$I_B = K_B \lambda_B \sin\theta \left[1 - \exp\left(-\frac{t_A}{\lambda_{BA}}\sin\theta\right)\right]$$

where λ_{BA} is the IMFP of B's electrons in material A, K_B is the above (but for photoelectrons of B), and, implicitly, $C_B = 1$. The intensities are ratioed to the total intensity of photoelectrons emitted from the sample and the assumption is made that the photoelectrons are of similar energy. This allows the K_i terms to be dropped.

For the multilayer case the general expression for the intensity of the photoelectrons of a certain species A from a particular layer j is as follows

$$I_{Aj} = \lambda_{Aj}^{AVE} \sin\theta \; C_{Aj}\left[1 - \exp\left(-\frac{t}{\lambda_{Aj}^{AVE}\sin\theta}\right)\right]\left[\Pi_{i=1}^{j-1} \exp\left(-\frac{t_i}{\lambda_{Ai}^{AVE}\sin\theta}\right)\right]$$

where C_{Aj} is the fractional concentration of species A in the jth layer; λ_{Aj}^{AVE} is the weighted average IMFP for photoelectrons of species A in the jth layer which equals

$$\sum_{n=1}^{NS} C_{nj}\lambda_{An} \quad \text{(NS is the total number of species)}$$

where C_{nj} is the concentration of species n in the jth layer and λ_{An} is the IMFP for the photoelectrons of species A in material of species n, and t_j is the thickness of the jth layer.

There are a number of factors that are assumed to be negligible in this model: (1) Reflection and refraction of electrons and X-rays, (2) electron diffraction, (3) elastic scattering of electrons, (4) asymmetric emission of electrons from sublevels, (5) surface roughness, and (6) λ = 2.5 nm for As and Ga 3d electrons based on recent calculations by Tanuma et al. (89)

BIOGRAPHICAL SKETCH

John T. Wolan, Jr., was born on November 2, 1957, in Abington, Pennsylvania, to John Thaddeus Wolan, Sr. and Ann Victoria Wolan. He attended Glenside Weldon Elementary School in Pennsylvania until 1971. At the age of 12, John relocated with his family to Orlando, Florida, where he attended Union Park Junior High School, then went on to Colonial High School graduating in 1975. John began his college education at the University of Central Florida in June of 1975, graduating in 1981 with a degree in secondary science education. At that time, he began teaching chemistry at Lake Brantly High School and remained there until August, 1989. John then decided to return to college as a graduate student in chemical engineering at the University of Florida. John currently performs research in surface science and semiconducting materials.

I certify that I have read this study and that in my opinion it conforms to acceptable standards of scholarly presentation and is fully adequate, in scope and quality, as a dissertation for the degree of Doctor of Philosophy

Gar B. Hoflund, Chairman
Professor of Chemical Engineering

I certify that I have read this study and that in my opinion it conforms to acceptable standards of scholarly presentation and is fully adequate, in scope and quality, as a dissertation for the degree of Doctor of Philosophy

Oscar D. Crisalle
Associate Professor of Chemical Engineering

I certify that I have read this study and that in my opinion it conforms to acceptable standards of scholarly presentation and is fully adequate, in scope and quality, as a dissertation for the degree of Doctor of Philosophy

Robert M. Park
Professor of Materials Science and Engineering

I certify that I have read this study and that in my opinion it conforms to acceptable standards of scholarly presentation and is fully adequate, in scope and quality, as a dissertation for the degree of Doctor of Philosophy

Lucy Elizabeth Seiberling
Professor of Physics

I certify that I have read this study and that in my opinion it conforms to acceptable standards of scholarly presentation and is fully adequate, in scope and quality, as a dissertation for the degree of Doctor of Philosophy.

Vaneica Y. Young
Associate Professor of Chemistry

This dissertation was submitted to the Graduate Faculty of the College of Engineering and to the Graduate School and was accepted as partial fulfillment of the requirements for the degree of Doctor of Philosophy

August 1998

Winfred M. Phillips
Dean, College of Engineering

Karen A. Holbrook
Dean, Graduate School